

Article

Reduced Siderite Ore Combined with Magnesium Oxide as Support Material for Ni-Based Catalysts; An Experimental Study on CO₂ Methanation

Kamonrat Suksumrit ¹, Christoph A. Hauzenberger ², Srett Santitharangkun ² and Susanne Lux ^{1,*}

¹ Institute of Chemical Engineering and Environmental Technology, Graz University of Technology, NAWI Graz, Inffeldgasse 25C, 8010 Graz, Austria; k.suksumrit@tugraz.at

² Department of Earth Sciences—NAWI Graz Geocenter, University of Graz, Universitätsplatz 2, 8010 Graz, Austria; christoph.hauzenberger@uni-graz.at (C.A.H.); srett.santitharangkun@edu.uni-graz.at (S.S.)

* Correspondence: susanne.lux@tugraz.at

Abstract: Ni-based catalysts play a fundamental role in catalytic CO₂ methanation. In this study, the possibility of using siderite ore as a catalyst or catalytic support material for nickel-based catalysts was investigated, aiming at the exploitation of an abundant natural resource. The catalytic performance of Ni-based catalysts with reduced siderite ore as a support was evaluated and compared to MgO as a support material. MgO is known as an effective support material, as it provides access to bifunctional catalysts because of its basicity and high CO₂ adsorption capacity. It was shown that undoped and Ni-doped reduced siderite ore have comparable catalytic activity for CO₂ hydrogenation (20–23%) at 648 K, but show limited selectivity toward methane (<20% for siderite_{reduced} and 60.2% for Ni/siderite_{reduced}). When MgO was added to the support material (Ni/siderite_{reduced}/MgO), both the CO₂ conversion and the selectivity toward methane increased significantly. CO₂ conversions were close to the thermodynamic equilibrium, and methane selectivities of ≥99% were achieved.

Keywords: CO₂ methanation; Ni-based catalyst; magnesium oxide; siderite ore



Citation: Suksumrit, K.; Hauzenberger, C.A.; Santitharangkun, S.; Lux, S. Reduced Siderite Ore Combined with Magnesium Oxide as Support Material for Ni-Based Catalysts; An Experimental Study on CO₂ Methanation. *Catalysts* **2024**, *14*, 206. <https://doi.org/10.3390/catal14030206>

Academic Editors: Chaoqiu Chen, Xin Jin, Xiao Chen, Jinshu Tian and Lihua Zhu

Received: 31 January 2024

Revised: 4 March 2024

Accepted: 15 March 2024

Published: 20 March 2024

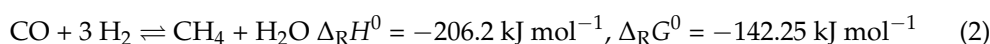


Copyright: © 2024 by the authors. Licensee MDPI, Basel, Switzerland. This article is an open access article distributed under the terms and conditions of the Creative Commons Attribution (CC BY) license (<https://creativecommons.org/licenses/by/4.0/>).

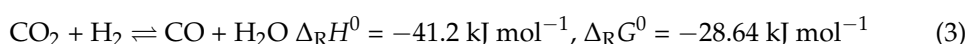
1. Introduction

Carbon dioxide (CO₂) is one of the major contributors to global climate change. To mitigate CO₂ emissions, increasing attention is directed to carbon capture and utilization (CCU) and carbon utilization (CU) technologies. These technologies aim at utilizing CO₂ from industrial processes as raw material for the production of value-added chemicals and fuels, for instance, methane (CH₄) [1–3], methanol (CH₃OH), and gasoline [4].

Methane synthesis by CO₂ hydrogenation has gained wide attention from researchers all over the world [5–7]. Methanation, referring to the conversion of carbon monoxide (CO) and/or carbon dioxide with hydrogen (H₂) into methane, is thermodynamically favorable (Equations (1) and (2)). Both reactions are highly exothermic; thus, high temperatures are unfavorable for the carbon oxide conversion [3,8,9].



Hydrogenation of CO₂ may also result in CO formation via the reverse water-gas shift reaction (Equation (3)).



To catalyze CO₂ methanation, ruthenium (Ru)- and rhodium (Rh)-based catalysts have shown promising catalytic activity and selectivity [10,11]. However, their high costs are

disadvantageous for industrial application. Currently, nickel (Ni)-based catalysts are the most widely used catalysts for CO₂ methanation because of their high catalytic activity, selectivity toward methane, and long-term stability. They help overcome the activation energy barrier, allowing the reaction to occur under mild conditions [12,13]. In addition, nickel is an abundant, relatively low-cost metal that helps extend the operational lifetime of the catalyst and thus reduces costs for catalyst replacement, which is crucial for industrial application. It is evident that the support material for the catalytically active nickel species has a pronounced effect on the activity and selectivity of the catalyst [14–18]. A series of different support materials for Ni-based catalysts is presented in the literature. Aluminum oxide (Al₂O₃), silicon dioxide (SiO₂), titanium dioxide (TiO₂), cerium oxide (CeO₂), and zirconium dioxide (ZrO₂), along with magnesium oxide (MgO), have been reported as support materials for Ni-based methanation catalysts [19–27]. Rahmani et al. produced a range of Ni catalysts supported on mesoporous nanocrystalline γ -Al₂O₃. The catalysts possessed large surface areas, with the 20 wt% Ni/Al₂O₃ catalyst showing the highest activity and stability between 473 K and 623 K [28]. Xu et al. investigated CO₂ methanation using Ni/SiO₂ catalysts that were prepared through a combustion-impregnation method and obtained a CO₂ conversion of 66.9% and a methane selectivity of 94.1% at 593 K [29]. However, the challenges encountered when using alumina and silica as support materials were carbon deposition and poor catalyst stability at the reaction temperatures [27,30]. Perkas et al. [31] developed Ni catalysts supported on mesoporous ZrO₂ modified with Ce and Sm cations, featuring 30 mol% Ni loading. These catalysts exhibited elevated catalytic activity for CO₂ methanation with a turnover frequency of 1.5 s⁻¹ at 573 K. Ni/ZrO₂ catalysts with various amounts of tetragonal polymorph ZrO₂ were prepared from an amorphous Ni-Zr alloy by Yamasaki et al. [32]. The tetragonal zirconia-supported nickel nanoparticles showed an even higher turnover frequency (TOF = 5.43 s⁻¹ at 473 K). Nevertheless, ZrO₂ and CeO₂ are expensive compared with other widely used support materials. Therefore, MgO has become an attractive alternative support material. Apart from being cost-effective, MgO has the significant advantages of exhibiting increased basicity of the surface, preventing catalyst deactivation, and mitigating issues of sintering and the formation of carbon deposits. Several studies have shown the efficiency and potential of MgO as a support material [33–35]. Ho et al. examined the CO₂ adsorption capability of MgO at various temperatures from 303 to 623 K [36]. As expected, with increasing temperatures, the CO₂ uptake capacity decreased. Takezawa et al. studied 13% Ni/MgO catalysts for CO₂ methanation. The catalysts were prepared by impregnation and calcination at temperatures of 673–973 K. The study revealed that with increasing calcination temperatures, the activity and selectivity of the Ni/MgO catalysts decreased. A methane selectivity of 98% was presented for catalyst calcination at 773 K followed by reduction at 873 K, a reaction temperature of 480 K, a pressure of 1 atm, and a feed gas flow rate of 10 mL min⁻¹ (CO₂:H₂ = 5:95) [37]. Varun et al. prepared NiO/MgO nanocomposite catalysts for CO₂ hydrogenation via sonochemical treatment and achieved a CO₂ conversion of 85%, with 98% selectivity toward methane at 673 K [38]. Baldauf-Sommerbauer et al. investigated two catalysts with 11 and 17 wt% Ni on MgO. The CO₂ conversion and methane selectivity approached the thermodynamic equilibrium at a moderate reaction temperature of 598 K and a feed composition of H₂:CO₂:N₂ = 4:1:5 at a feed gas flow rate of 250 mL_{STP} min⁻¹ [39]. Loder et al. investigated the effect of the Ni loading (0–27 wt%) on MgO and the MgO quality on the rate of CO₂ methanation in a temperature range of 533–648 K. They reported CO₂ conversions of 87% and a methane selectivity of $\geq 99\%$ [9]. In a current review, the role of carbonate formation during CO₂ hydrogenation over MgO-supported catalysts was discussed, explicitly stating the beneficial effect of bifunctional Ni/MgO catalysts toward methane synthesis [40]. In the case of Ni/MgO catalysts, nickel provides the adsorbent capacity for hydrogen and is highly selective for methane, whereas the basic support material, MgO, activates CO₂ through chemisorption, giving access to a highly active bifunctional catalyst.

In addition, Pandey et al. showed that adsorbed carbonate species on iron oxide sites on Ni-Fe catalysts serve as additional factors that enhance the efficiency of catalysts for CO₂ hydrogenation. The presence of a Ni-Fe alloy and a number of metal sites were reported to enhance CO₂ conversion and methane yield [41]. In general, iron-based catalysts were suggested as a cost-effective alternative for methane synthesis from CO₂, providing long-term stability when appropriately combined and modified with promoters [42]. Sehested et al. confirmed that a Ni-Fe alloy catalyst gave higher CO₂ conversion and CH₄ selectivity compared with a pure nickel catalyst at 603 K with excess hydrogen [43]. Mutz et al. studied the potential of Ni₃Fe on γ -Al₂O₃ as a methanation catalyst in a microchannel packed bed reactor. With a 17% Ni₃Fe catalyst, a CO₂ conversion of 71% and a selectivity toward methane > 98% were achieved at 631 K and 6 bar in long-term experiments (45 h). Thus, the Ni₃Fe catalyst showed outstanding performance and stability at mid-temperatures when combining Ni and Fe [44]. In addition, Serrer et al. investigated bimetallic Ni_{3.2}Fe/Al₂O₃ catalysts by using an advanced combination of operando XAS and XRD with quantitative on-line product analysis. The results showed that Fe addition to Ni/Al₂O₃ catalysts protected active Ni⁰ species from oxidation and preserved the catalytic activity under dynamic reaction conditions [45]. Mebrahtu et al. studied Ni-Fe bimetallic catalysts on a (Mg,Al)O_x support, which were synthesized by co-precipitation. Ni-Fe alloy nanoparticles were favorable for the methanation of CO₂. The activity and selectivity were remarkably affected by iron, attributable to its small particle size, facilitated CO dissociation, and tailored surface basicity. With the best catalyst (Fe/Ni = 0.1), the CO₂ conversion rate was 6.96 mmol CO₂ mol_{Fe+Ni}⁻¹ s⁻¹ at 608 K, with a consistent selectivity of 99.3% toward CH₄ over 24 h on stream [46]. In contrast, Wang et al. used calcined olivine ((Mg, Fe)₂SiO₄) as support for Ni catalysts that were prepared by the incipient wetness method, and applied them for CO₂ methanation. The results showed that a FeO_x phase was formed on the surface of the calcined olivine and that the unreduced FeO_x between the active Ni-Fe alloy phase and the olivine support played a crucial role in CO₂ methanation. A 98% CO₂ conversion and a selectivity of 99% toward CH₄ were achieved at a temperature of 673 K, a H₂/CO₂ molar ratio of 6, and an hourly space velocity of 11,000 h⁻¹ [47].

Table 1 gives a list of experimental studies with Ni- and Fe-based catalysts on different support materials for CO₂ methanation.

Table 1. Experimental studies with Ni- and Fe-based catalysts on different support materials for CO₂ methanation.

Catalyst Composition	Preparation Method	Operation Conditions	Performance	Ref.
Ni/MgO ($w_{\text{Ni}} = 0\text{--}27$ wt%)	wet impregnation	$T = 533\text{--}648$ K GHSV = $3.7 \text{ m}^3 \text{ kg}^{-1} \text{ h}^{-1}$ H ₂ :CO ₂ :N ₂ = 4:1:5	$X_{\text{CO}_2} = 87\%$ $S_{\text{CH}_4} = 99\%$	[9]
Mg-Al-CO ₃ LDH ¹ catalyst	coprecipitation	$T = 473\text{--}573$ K CO ₂ :O ₂ :N ₂ = 14:4:82	CO ₂ sorption: 2.72% (dry sorption), 3.14% (wet condition, 12% water)	[48]
Ni/CeO ₂	wet impregnation	$T = 573$ K $F = 3000 \text{ mL min}^{-1}$	$X_{\text{CO}_2} > 90\%$ $S_{\text{CH}_4} > 99.5\%$	[49]
Ni/Al ₂ O ₃ SiO ₂	sol-gel	$T = 625$ K H ₂ :CO ₂ = 3.5:1 GHSV = $12,000 \text{ mL g}^{-1} \text{ h}^{-1}$	$X_{\text{CO}_2} = 77\%$ $S_{\text{CH}_4} = 98\%$	[50]
Ni/ZrO ₂ , Ni-K/ZrO ₂ and Ni-La/ZrO ₂	wetness impregnation	$T = 523\text{--}723$ K H ₂ :CO ₂ = 12.5:1 $F = 50\text{--}100 \text{ mL min}^{-1}$	$X_{\text{CO}_2} = 20\text{--}60\%$ $S_{\text{CH}_4} = 89\text{--}99\%$	[51]

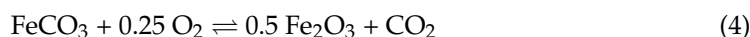
Table 1. Cont.

Catalyst Composition	Preparation Method	Operation Conditions	Performance	Ref.
Ni-FeAl-(NH ₄) ₂ CO ₃	co-precipitation	T = 493 K CO ₂ :H ₂ :N ₂ = 1:4:1.7 WHSV = 9600 mL g ⁻¹ h ⁻¹	X _{CO₂} = 58.5% S _{CH₄} = 64%	[52]
Ni/MCM-41 with VO _x -modified		T = 673 K WHSV = 60,000 mL g ⁻¹ h ⁻¹	X _{CO₂} = 81.4% S _{CH₄} = 72.8%	[53]
Ni-Fe/S16	mesoporous silica molecular sieve	T = 473–573 K H ₂ :CO:N ₂ = 3:1:1 WHSV = 15,000 mL g ⁻¹ h ⁻¹	X _{CO} = 100% (at 503 K) S _{CH₄} > 90%	[54]
Ni-Fe/olivine ((Mg _x Fe _{1-x}) ₂ SiO ₄)	wet impregnation	T = 673 K H ₂ :CO ₂ = 6:1 GHSV = 11,000 h ⁻¹	X _{CO₂} = 98% S _{CH₄} = 99%	[47]
1–10 wt% Fe/13X	wet impregnation	T = 473–823 K P = 1–15 bar	X _{CO₂} = 74% (T = 823 K, P = 15 bar) S _{CH₄} = 76% (P = 5–15 bar)	[42]
10Ni-Fe/C _{A-C} ²	wet impregnation	T = 473–773 K H ₂ :CO ₂ = 4:1 GHSV = 12,000 h ⁻¹	X _{CO₂} = 5–74% S _{CH₄} > 90%	[55]
γ-Fe ₂ O ₃ (n) and	commercial from Sigma-Aldrich	T = 523–723 K H ₂ :CO ₂ = 4:1 F = 500 mL min ⁻¹ GHSV = 120,000 h ⁻¹	X _{CO₂} = 45–65% (65% at 723 K) S _{CH₄} = 45–77% (77% at 623 K)	[56]
α-Fe ₂ O ₃ (PVA)	polyvinyl alcohol (PVA) route	T = 523–723 K H ₂ :CO ₂ = 4:1 F = 500 mL min ⁻¹ GHSV = 120,000 h ⁻¹	X _{CO₂} = 96% (723 K) S _{CH₄} = 11% (673 K)	

¹ layered double hydroxide, ² C is a carbon support.

In several studies, iron-bearing materials, for instance, iron-bearing minerals such as siderite ore (FeCO₃), were used for catalyst preparation for a variety of applications and processes [56–59]. For instance, Hadjiltaief et al. studied two natural samples, natural Tunisian hematite and siderite, as catalysts for the photocatalytic degradation of 4-chlorophenol (4-CP) in aqueous solution. Siderite exhibited higher photocatalytic oxidation activity than hematite at pH 3. Use of the siderite catalyst gave 100% conversion of 4-CP and 54% TOC removal. In terms of the removal of several organic compounds in an aqueous condition, the work confirmed that natural materials can be used as catalysts [60]. Wei et al. used siderite (doped with Mn and Ce) for the selective catalytic reduction (SCR) of NO_x by NH₃. The siderite catalysts showed high efficiency for the removal of NO_x (NO_x conversions were higher than 90% at T = 513–573 K and T_{calculated} = 723 K). A 3% Mn/1% Ce-siderite catalyst also showed high resistance against sulfur poisoning (the NO_x conversion remained above 75% after introducing 0.01% SO₂ in the feed for 7.5 h) [61]. Furthermore, Görmez et al. studied the use of rhombohedral FeCO₃ that was synthesized hydrothermally as a catalyst in the electro-fenton oxidation of *p*-benzoquinone. 95% of the total organic carbon was removed at 400 mA current. Increasing catalyst dosage had a beneficial effect on the mineralization of *p*-benzoquinone [62].

These studies show the beneficial catalytic effect of iron in various aspects and highlight its use by exploiting natural iron resources as abundant catalysts or catalyst support materials. Siderite ore, for instance, is an important source for iron and steel production in Austria [63] and China [64]. In general, siderite ore is converted to blast furnace-grade hematite through roasting in air in the sinter plant (Equation (4)).



In the context of decarbonizing iron and steel production, a novel direct reduction process (Equation (5)) for siderite ore with hydrogen was developed, which can be combined with subsequent catalytic CO₂ hydrogenation [65–67].



It was shown that during the direct reduction process, not only is CO₂ released from the carbonaceous ore, but also CO and methane are formed [65]. Moreover, Bock et al. suggested the application of this inexpensive and abundant natural siderite ore for energy storage with combined hydrogen and heat release [68].

The above-stated publications clearly show the beneficial effect of iron during CO₂ methanation and the potential of using natural iron-bearing minerals with regard to catalysis. Methane formation during the direct reduction of siderite ore suggests that this iron ore has a certain catalytic effect on CO₂ methanation. However, its potential as a catalyst for CO₂ methanation has not been evaluated yet. This raises the question of whether siderite ore can be considered a catalyst or catalyst support material for Ni-based catalysts for CO₂ methanation. For this purpose, Ni-based catalysts on MgO as a support material may act as benchmark catalysts in this study. The advantageous effect of MgO as a support material for nickel catalysts in CO₂ methanation has already been described. This in turn raises the question of whether the catalytic performance of Ni/MgO catalysts can be increased by adding siderite ore, which could create synergies and provide iron species acting as catalyst promoters.

Thus, the aim of this study was to investigate the potential of abundantly available siderite ore as a cheap raw material source for catalyst production for CO₂ methanation. Both its sole catalytic effect and a possible synergistic effect with MgO as a support material for Ni-based catalysts were considered. For this purpose, in a hydrogen atmosphere reduced siderite ore with and without nickel doping was used. Furthermore, the interplay of mixed reduced siderite ore/MgO support materials was examined, possibly opening a path to abundant, inexpensive bifunctional catalysts for CO₂ methanation.

2. Results and Discussion

The catalytic performance of hydrogen-reduced siderite ore for CO₂ hydrogenation to methane was investigated. The use of unreduced siderite ore is not reasonable, as otherwise CO₂ would constantly be released from the ore during the hydrogenation reaction, which would change the catalyst composition and its properties during the process.

In addition, the catalytic effect of Ni-based catalysts on support materials of MgO and siderite ore reduced with hydrogen prior to their application was evaluated. The process conditions were chosen based on the work of Sommerbauer et al. [39] and Loder et al. [9]. The molar feed gas ratio of CO₂:H₂ was 4:1. Inert nitrogen was added to the feed gas stream for balancing purposes (H₂:CO₂:N₂ = 56:14:30). From the literature it can be deduced that the availability of adsorbed hydrogen is a limiting factor for the rate of reaction of CO₂ methanation. Loder et al. investigated this effect and varied the H₂:CO₂ ratio in the feed gas from 3:1 to 5:1 [9]. As expected, the CO₂ conversion rose with rising hydrogen concentrations in the feed gas stream, yielding a maximum CO₂ conversion of 98% (equilibrium conversion: 99.8%) for the H₂:CO₂ ratio of 5:1. However, as most of the experiments in the study of Loder et al. were performed with a stoichiometric feed gas ratio of CO₂:H₂ = 4:1, for reasons of comparability, this ratio was also chosen in this study.

The performance of the different catalysts for CO₂ methanation was investigated at temperatures of 548 K, 598 K, and 648 K, and feed gas flow rates of 8.02, 11.32, and 14.66 m³ kg⁻¹ h⁻¹ (STP), referring to the flow rate of the feed gas stream per mass of catalyst.

To provide a baseline reference, the catalytic effect of the support material MgO was also tested and compared to the undoped, reduced siderite ore. Then, both—in hydrogen-reduced siderite ore and MgO—were used as support materials and were doped with Ni in various amounts (Ni loading from 22 to 31 wt%).

2.1. Catalytic Effect of Reduced Siderite Ore and MgO

As a baseline reference, the catalytic effect of hydrogen-reduced siderite ore was studied and compared to the catalytic performance of undoped MgO for CO₂ hydrogenation at 548 K, 598 K, and 648 K, respectively.

For the reduced siderite ore, siderite ore was reduced in a hydrogen atmosphere at two different reduction temperatures (T_{red}): 773 K and 973 K, respectively. The reduced ore was then removed from the reactor and kept at atmospheric conditions so that it was partially reoxidized and reached a stable state at atmospheric conditions. After that, the reduced ore was filled back into the reactor to perform the CO₂ hydrogenation experiments. The effect of the reduction temperature during siderite ore reduction was then evaluated regarding the characteristics of the support material during CO₂ hydrogenation.

For the undoped MgO catalyst, undoped MgCO₃ was prepared as described in Section 3.1, with the MgCO₃ being calcined in a muffle furnace with air at 723 K for 2 h and at 823 K for a further 5 h.

The CO₂ hydrogenation was carried out with the help of the undoped materials at different feed gas flow rates (8.02, 11.32, and 14.66 m³ kg⁻¹ h⁻¹) and a constant feed gas ratio of H₂:CO₂:N₂ = 56:14:30, and at reaction temperatures of 548 K, 598 K, and 648 K, respectively. The reaction temperatures were chosen because temperatures below 700 K are known to promote CO₂ methanation over CO formation from CO₂ [9].

2.1.1. Reduced Siderite Ore as a Catalyst

First, the catalytic effect of reduced siderite ore was proven for methane formation from CO₂. As depicted in Figure 1, the reduction temperature of siderite ore influences its performance during CO₂ hydrogenation, both regarding CO₂ conversion (a) and selectivity toward CH₄ (b). When the CO₂ hydrogenation was carried out at temperatures of 548 K and 598 K, the CO₂ conversion was below 5%, and the two siderite ore samples, that were reduced at different temperatures, showed no clear difference regarding their catalytic effect. At a reaction temperature of 648 K, the siderite ore sample that was reduced at $T_{\text{red}} = 973$ K showed a pronounced catalytic effect, yielding CO₂ conversions of 12–15%. At all reaction temperatures, the siderite ore samples that were reduced at $T_{\text{red}} = 973$ K gave higher CH₄ selectivities: 19.0% at 548 K and 5% at 598 K and 648 K, respectively. Compared with siderite ore reduction at $T_{\text{red}} = 773$ K, the higher reduction temperature of $T_{\text{red}} = 973$ K enhanced both the CO₂ conversion and the selectivity toward CH₄. At $T_{\text{red}} = 973$ K, at the lowest feed gas flow rate (8.02 m³ kg⁻¹ h⁻¹), which meant the highest residence time in the reactor, the highest CO₂ conversion (19.9%) was obtained, while the highest CH₄ selectivity (19.0%) was obtained at the higher feed gas flow rates (11.32–14.66 m³ kg⁻¹ h⁻¹). Since the effect of increasing methane selectivity with increasing feed gas flow rate and thus lower residence time was only observed at the lowest reaction temperature of 548 K and only the methane selectivity at a feed gas flow rate of 8.02 m³ kg⁻¹ h⁻¹ differed from the one at 11.32 and 14.66 m³ kg⁻¹ h⁻¹, respectively, it is assumed that this value should rather be regarded as an outlier.

As the reaction temperature increased, the CH₄ selectivity decreased. CO was formed instead, showing that the reverse water-gas shift reaction was the dominant reaction. This is consistent with the findings of Lux et al., who investigated the direct reduction process of siderite ore with hydrogen, called reductive calcination in the study, with the aim of optimizing the process parameters to maximize the methane yield. Since it can be assumed that CO₂ is released from iron carbonate during direct reduction with hydrogen in a first step, and is further reduced to methane in a subsequent catalytic step, the results are directly transferable. As expected, in their study, it was proven that methane formation is favored at low temperatures and increased pressure, whereas the formation of CO is favored at high temperatures and low pressure [67].

The direct reduction of siderite ore with hydrogen has been extensively investigated for iron production. Loder et al., for instance, investigated the reaction kinetics and gave a detailed report on the degree of metallization (=mass of elemental iron per total mass of iron

in the reduced ore) for different reduction temperatures under atmospheric conditions [66]. The direct reduction experiments were carried out with the same original siderite ore from the Styrian Erzberg, with a feed gas ratio of $\text{H}_2:\text{CO}_2:\text{N}_2 = 56:14:30$ and a feed gas flow rate of $0.05 \text{ m}^3 \text{ h}^{-1}$ (STP) ($=0.0083 \text{ m}^3 \text{ kg}^{-1} \text{ min}^{-1}$ (STP)) at ambient pressure. The effect of the reduction temperature was investigated in a temperature range of 773–1023 K. After the reduction experiments, the reduced ore was removed from the reactor under inert nitrogen conditions and analyzed for its degree of metallization. At a reduction temperature of 773 K, the degree of metallization of the reduced ore was 40%. At a reduction temperature of 973 K, a degree of metallization of 89% was obtained.

As the handling of catalysts under ambient conditions in air is easier and the impregnation of the reduced ore requires handling under ambient conditions and exposure to the solution anyway, the behavior of the reduced siderite ore when exposed to air was evaluated in this study. For this purpose, the same direct reduction experiments were carried out, but the removal of the reduced ore from the reactor was done under ambient conditions in air as compared to emptying the reactor and keeping the reduced siderite ore under an inert nitrogen atmosphere. For a reduction temperature of 973 K, this resulted in a partial reoxidation of the reduced iron species and thus a reduced degree of metallization of 58.2%, as compared with 89% under inert nitrogen conditions. The remaining iron fraction was split up into 32.6% Fe^{2+} and 9.1% Fe^{3+} for the partially reoxidized reduced siderite ore sample. This means that the majority of iron was present as metallic iron Fe^0 (58.2%) together with smaller fractions of Fe^{2+} (32.6%) and Fe^{3+} (9.1%) when siderite ore was reduced in a hydrogen atmosphere at 973 K and finally kept under ambient conditions in air. The determination of the chemical composition of the reduced (and partially oxidized) siderite ore samples is described in Section 3.4.3.

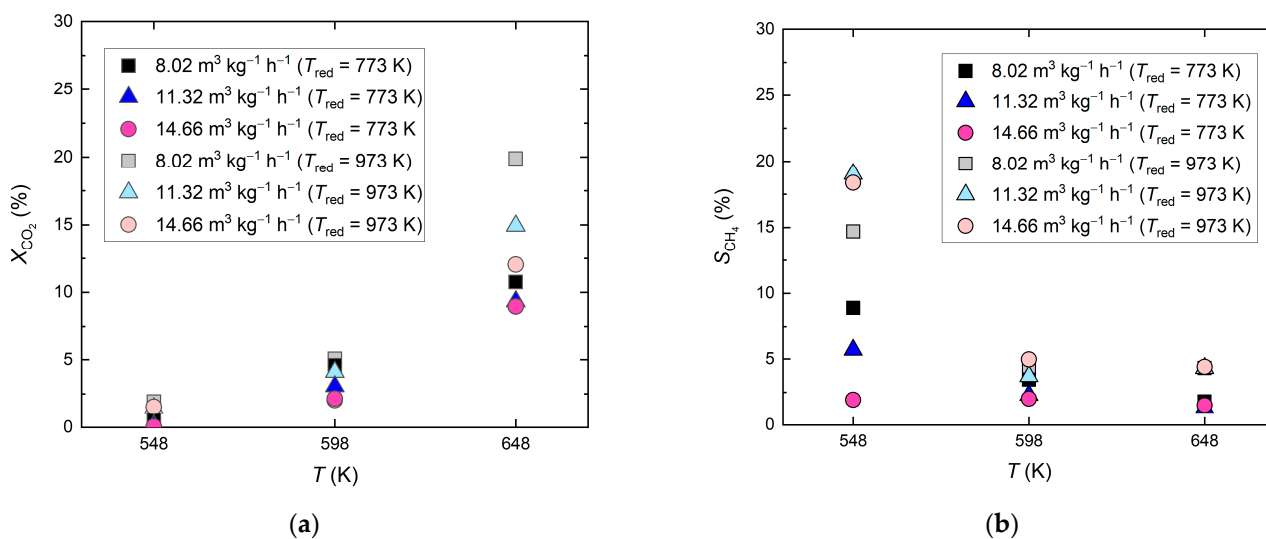


Figure 1. Catalytic effect of reduced siderite ore during CO_2 hydrogenation; reduction of siderite ore in hydrogen atmosphere at $T_{\text{red}} = 773 \text{ K}$ and 973 K ; molar feed gas ratio $\text{H}_2:\text{CO}_2:\text{N}_2 = 56:14:30$, feed gas flow rate $8.02\text{--}14.66 \text{ m}^3 \text{ kg}^{-1} \text{ h}^{-1}$ (STP), reaction temperatures 548–648 K; (a) CO_2 conversion and (b) CH_4 selectivity.

To conclude, two different reduction temperatures ($T_{\text{red}} = 773$ and 973 K) were studied for the preparation of the reduced siderite ore via direct reduction with hydrogen in a tubular reactor under ambient pressure. The reduction temperature was chosen according to suggestions in the literature for direct reduction of siderite ore [65,66]. Via this procedure, CO_2 was released from the ore, and the carbonaceous iron ore was reduced to elemental iron with minor remaining fractions of Fe^{2+} and Fe^{3+} . When exposed to air under ambient conditions, the reduced siderite ore was partially oxidized, and for the siderite ore reduced at 973 K, more than half of the iron was still present as metallic iron Fe^0 (58.2%), together

with smaller fractions of Fe^{2+} (32.6%) and Fe^{3+} (9.1%). The degree of metallization strongly depends on the reduction temperature. Furthermore, reduction at higher temperatures results in a reduced iron ore that is more chemically stable against reoxidation. When reduced siderite ore was used as the sole catalyst for CO_2 hydrogenation/methanation, higher CO_2 conversions were obtained with the siderite ore that was reduced at the higher reduction temperature of 973 K. This may be attributed to the higher fraction of metallic iron in the reduced siderite ore. However, CO_2 conversions were comparably low, as the maximum CO_2 conversion was around 20%, and the selectivity toward methane even remained below 20%.

2.1.2. Undoped MgO

Second, undoped MgO was used for CO_2 hydrogenation in the same reaction conditions as with the reduced siderite ore. In this case, CO_2 was hardly converted. CO_2 conversions were below 0.7%, as depicted in Figure 2. Methane was not detected in the product gas.

The catalytic effect of MgO during CO_2 hydrogenation was already reported by Loder et al. [9], who postulated that MgO shows minor catalytic activity for the reverse water-gas shift reaction but does not promote methane formation [9]. This was confirmed by the findings in this work.

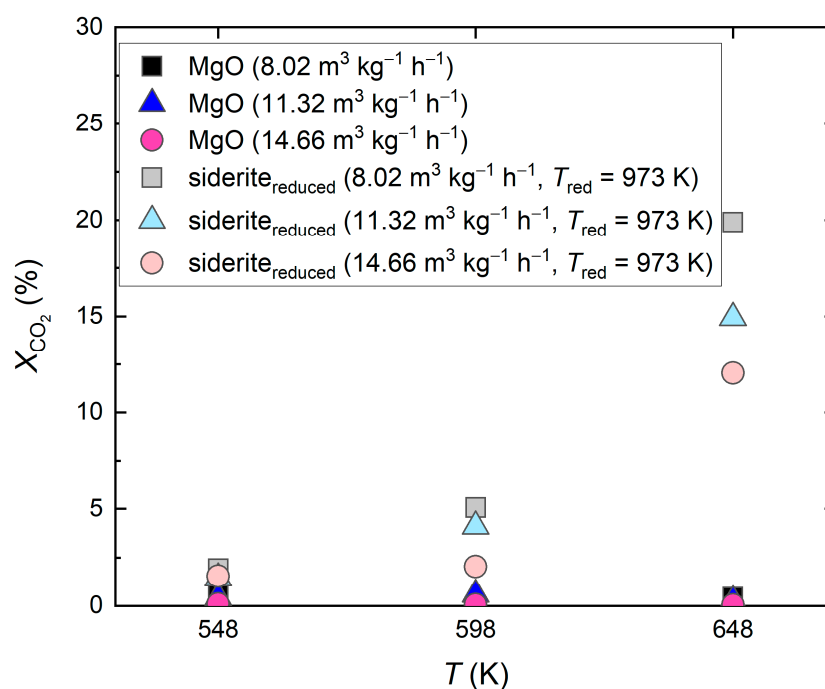


Figure 2. Catalytic effect of undoped MgO and reduced siderite ore (siderite_{reduced}) during CO_2 hydrogenation; reduction of siderite ore in hydrogen atmosphere at $T_{\text{red}} = 973$ K; molar feed gas ratio $\text{H}_2:\text{CO}_2:\text{N}_2 = 56:14:30$, feed gas flow rate $8.02\text{--}14.66$ m^3 kg^{-1} h^{-1} (STP), reaction temperatures 548–648 K.

2.2. Ni-Based Catalysts on Reduced Siderite Ore as Support Material

Next, siderite ore reduced in a hydrogen atmosphere was studied as a support material for Ni-based catalysts (Figure 3). As undoped siderite ore that was reduced at $T_{\text{red}} = 973$ K had shown a pronounced catalytic effect during CO_2 hydrogenation as compared with the siderite ore that was reduced at $T_{\text{red}} = 773$ K, a reduction temperature of T_{red} of 973 K was chosen for siderite ore reduction in hydrogen prior to loading with nickel.

The effect of Ni loading was investigated at different reaction temperatures and feed gas flow rates at ambient pressure. Ni loading was varied from 22 wt% Ni (Figure 3a) to 24 wt% Ni (Figure 3b), 25 wt% Ni (Figure 3c), and 27 wt% Ni (Figure 3d) for feed gas flow

rates of 8.02, 11.32, and 14.66 $\text{m}^3 \text{kg}^{-1} \text{h}^{-1}$, and reaction temperatures of 548 K, 598 K, and 648 K.

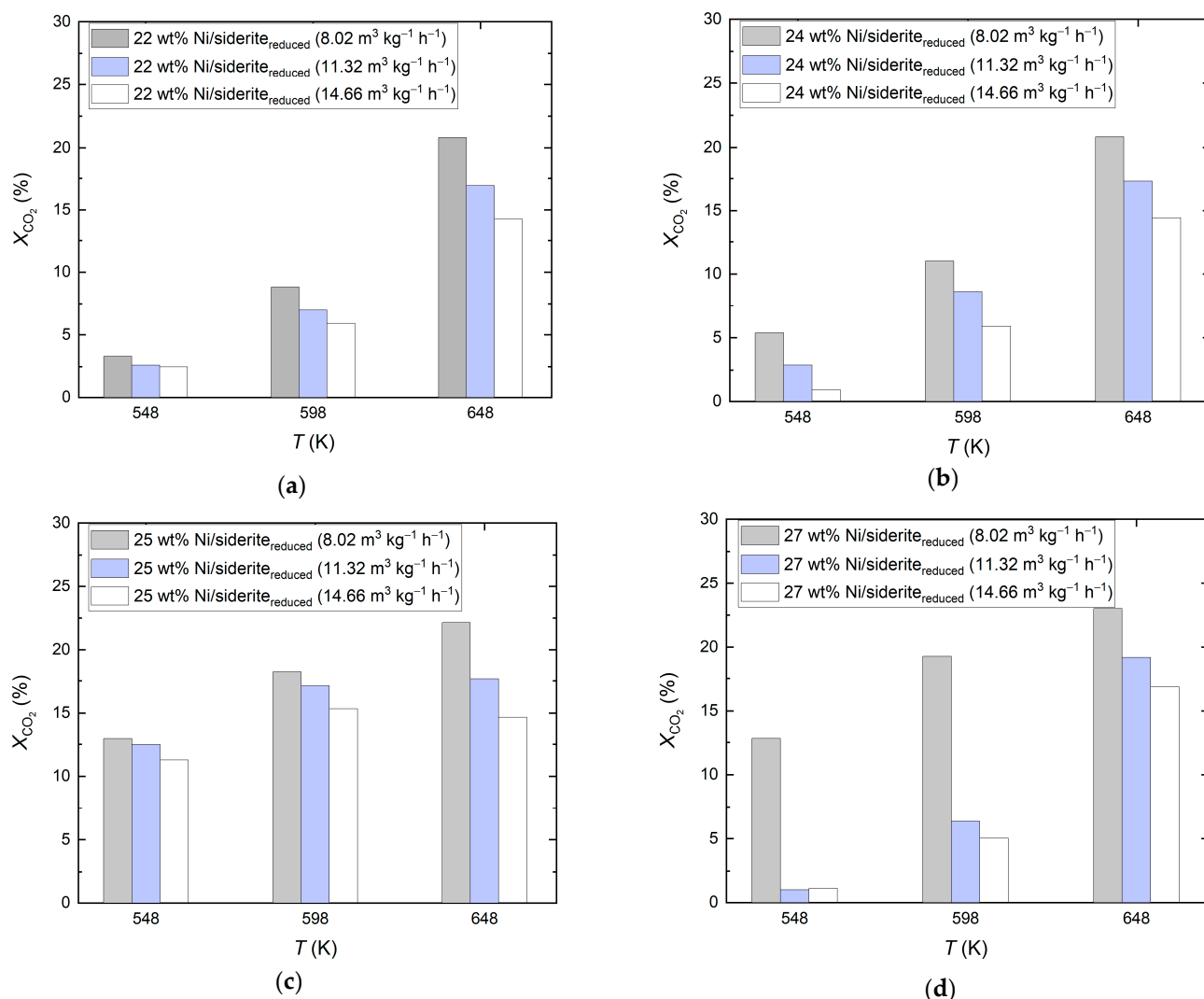


Figure 3. Catalytic performance of Ni-based catalysts on reduced siderite ore as support material during CO₂ hydrogenation; molar feed gas ratio H₂:CO₂:N₂ = 56:14:30, feed gas flow rate 8.02–14.66 $\text{m}^3 \text{kg}^{-1} \text{h}^{-1}$ (STP), reaction temperature 548 K, 598 K, and 648 K; (a) 22 wt% Ni/siderite_{reduced}, (b) 24 wt% Ni/siderite_{reduced}, (c) 25 wt% Ni/siderite_{reduced}, and (d) 27 wt% Ni/siderite_{reduced}.

For all Ni loadings of the Ni/siderite_{reduced} catalysts, the CO₂ conversion increased with increasing reaction temperature and decreasing feed gas flow rate (increasing residence time). The highest CO₂ conversion was 23.8% and was obtained with the 27 wt% Ni/siderite_{reduced} catalyst at a reaction temperature of 648 K. The effect of Ni loading on the CO₂ conversion and the CH₄ selectivity at a constant feed gas flow rate of 8.02 $\text{m}^3 \text{kg}^{-1} \text{h}^{-1}$ is depicted in Figure 4. Both the CO₂ conversion and the CH₄ selectivity increased with increasing Ni loading. At reaction temperatures of 548 K and 598 K, the CO₂ conversion increased significantly with increasing Ni loading from 22 wt%/24 wt% to 25 wt%, but only slightly increased further for a Ni loading of 27 wt%. At a reaction temperature of 648 K, only a minor effect of Ni loading on the CO₂ conversion was visible. As opposed to the findings with undoped support material, with increasing reaction temperatures, the selectivity toward CH₄ increased.

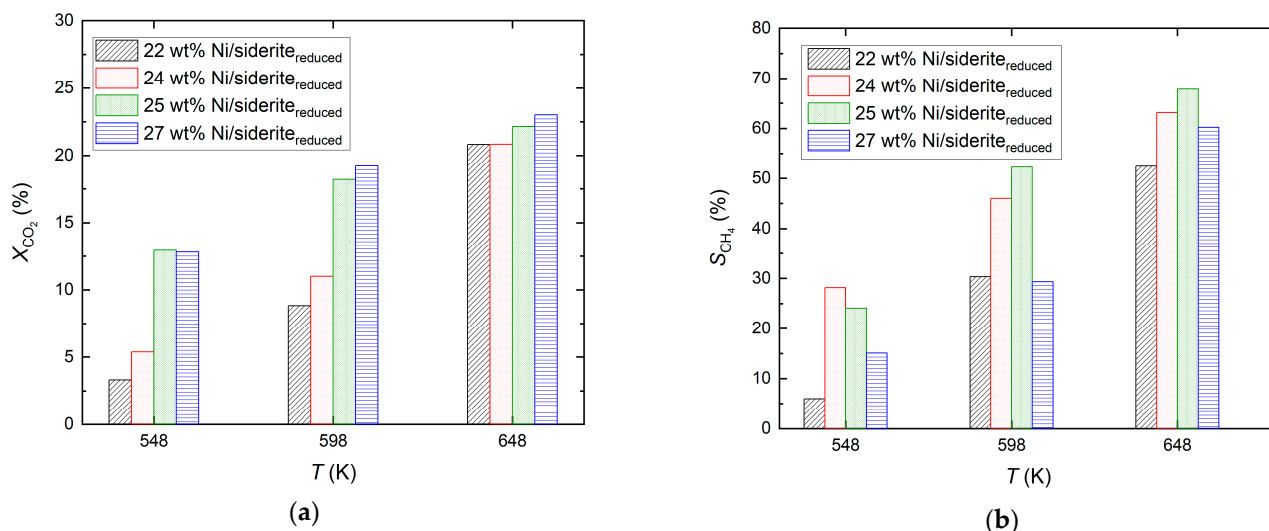


Figure 4. Effect of Ni loading of Ni/siderite_{reduced} catalysts on CO₂ conversion (a) and selectivity toward CH₄ (b) during CO₂ hydrogenation; molar feed gas ratio H₂:CO₂:N₂ = 56:14:30, feed gas flow rate 8.02 m³ kg⁻¹ h⁻¹ (STP), reaction temperatures 548 K, 598 K, and 648 K.

The catalytic activity of the 27 wt% Ni/siderite_{reduced} catalyst adopts an exceptional position in the range of Ni/siderite_{reduced} catalysts. Its catalytic activity in terms of CO₂ conversion is only marginally higher than that of the 25 wt% Ni/siderite_{reduced} catalyst. At all three reaction temperatures, however, it shows a significantly reduced selectivity for methane. Furthermore, the 27 wt% Ni/siderite_{reduced} catalyst shows poor catalytic activity when the feed gas flow rate is high and, thus, the residence time is low. This suggests that in this range, a maximum Ni load is present, which is advantageous in terms of methane selectivity. Furthermore, it must be noted that the production of catalysts with such a high Ni loading on reduced siderite ore is more difficult to reproduce, which could also be reflected in the experimental results. However, at low feed gas flow rates (Figure 4), the catalyst with the highest Ni loading (27 wt% Ni/siderite_{reduced}) gave the highest CO₂ conversion (23.0%) and high CH₄ selectivity (60.2%). Thus, a high Ni loading (26–28 wt% Ni) was chosen in the subsequent study to investigate the catalytic performance of Ni-based catalysts on mixed reduced siderite ore/MgO support material.

2.3. Mixed Reduced Siderite Ore/Magnesium Oxide as Support Material for Ni-Based Catalysts

In previous studies, MgO has already been proven to be an effective support material for Ni-based catalysts, giving access to bifunctional Ni/MgO catalysts [9,39]. In this study, a 31 wt% Ni/MgO catalyst was prepared and used as a benchmark catalyst.

In order to test the catalytic performance of mixed MgO and reduced siderite ore as support materials for Ni-based catalysts, various ratios of reduced siderite ore and MgO were tested at constant Ni loading of 28 wt%; siderite_{reduced}/MgO (*w/w*) = 30:70, 50:50, and 70:30, respectively.

As depicted in Figure 5, Ni/siderite_{reduced}/MgO catalysts efficiently catalyze CO₂ hydrogenation. As expected, for all three catalysts—siderite_{reduced}/MgO = 30:70, 50:50, 70:30—the CO₂ conversion increases with increasing reaction temperature and decreasing feed gas flow rate. The highest CO₂ conversions were obtained with the catalysts with a higher fraction of reduced siderite (siderite_{reduced}/MgO = 50:50, 70:30), with CO₂ conversions of 74.2–78.0%, 67.0–69.95%, and 63.5–65.8% at a reaction temperature of 648 K and feed gas flow rates of 8.02, 11.32, and 14.66 m³ kg⁻¹ h⁻¹, respectively.

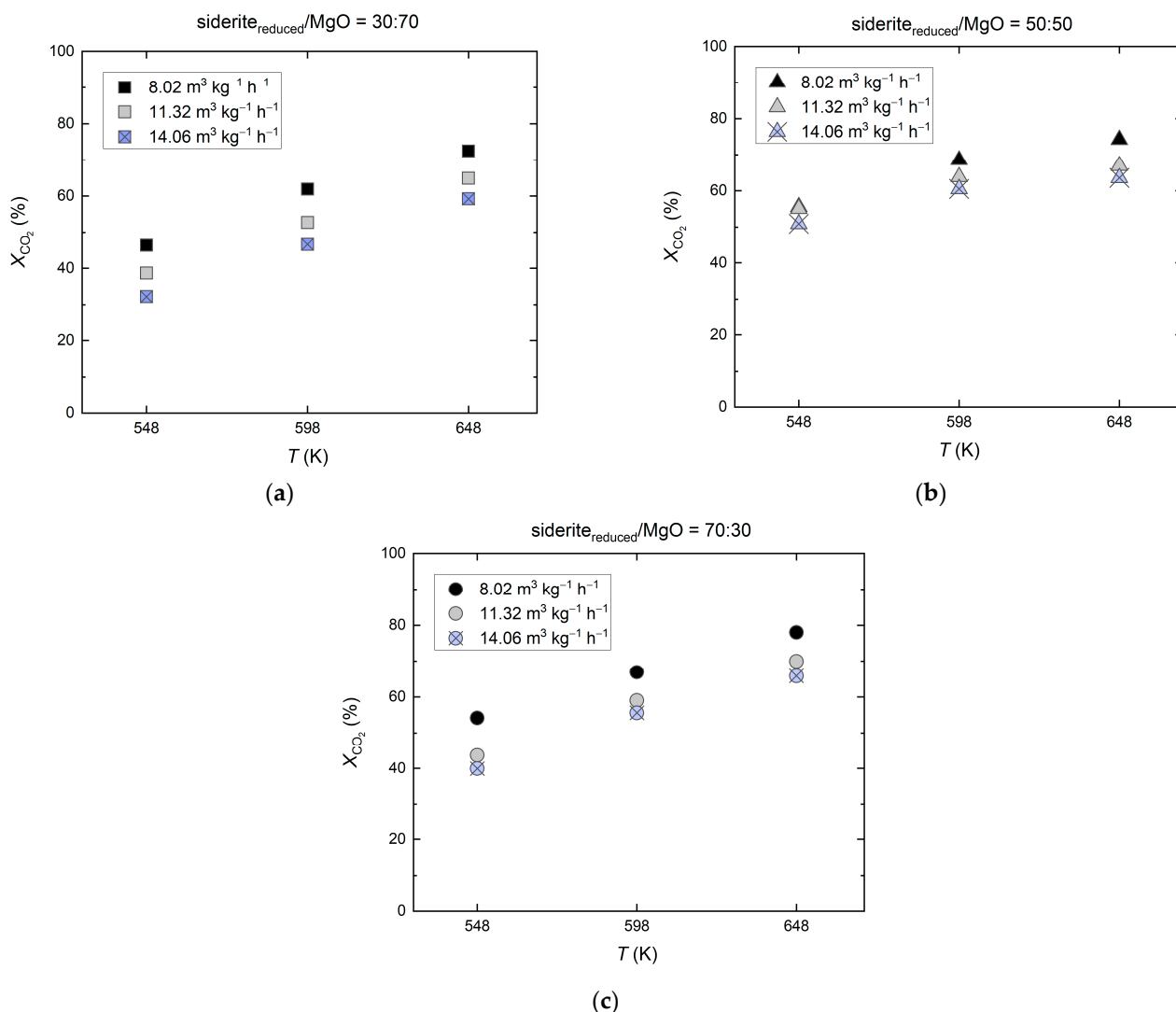


Figure 5. Catalytic performance of Ni-based catalysts (28 wt% Ni) on mixed siderite_{reduced}/MgO support material in various compositions for CO₂ hydrogenation; molar feed gas ratio H₂:CO₂:N₂ = 56:14:30, feed gas flow rate 8.02–14.66 m³ kg⁻¹ h⁻¹ (STP), reaction temperatures 548–648 K, reduction of siderite ore in hydrogen at $T_{\text{red}} = 973$ K; (a) siderite_{reduced}/MgO = 30:70, (b) siderite_{reduced}/MgO = 50:50, and (c) siderite_{reduced}/MgO = 30:70.

Figure 6 depicts the catalytic performance of the 28 wt% Ni/siderite_{reduced}/MgO catalysts compared with Ni-based catalysts on MgO (31 wt% Ni/MgO) or reduced siderite ore (28 wt% Ni/siderite_{reduced}) only. It is evident that the Ni/siderite_{reduced} catalyst performed the worst. When MgO was added to the support material, there was a clear improvement in catalytic performance. At lower reaction temperatures (548 K), the catalytic performance seemed to be worse with an excess of MgO (siderite_{reduced}/MgO = 30:70) in the support material compared with the catalysts with lower MgO fractions (siderite_{reduced}/MgO = 50:50, 70:30). However, the difference was small and seemed to be canceled out at higher temperatures (648 K). No difference was visible for the Ni/siderite_{reduced}/MgO catalysts with reduced siderite ore to MgO mass ratios of 50:50 and 70:30. CH₄ selectivities were >95% with all Ni/siderite_{reduced}/MgO catalysts.

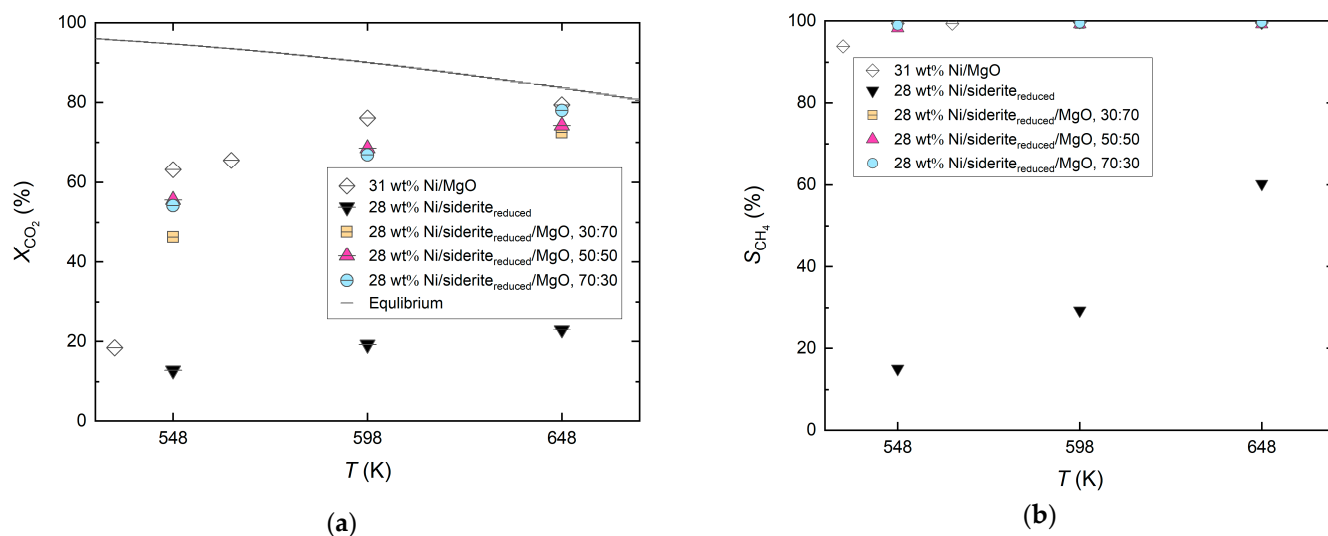


Figure 6. Comparison of the catalytic performance of Ni-based catalysts on reduced siderite ore, MgO, and mixed reduced siderite ore/MgO support material (27–30 wt% Ni) for various reaction temperatures (548–648 K); molar feed gas ratio H₂:CO₂:N₂ = 56:14:30, feed gas flow rate 8.02 m³ kg⁻¹ h⁻¹ (STP), reduction of siderite ore in hydrogen at $T_{red} = 973$ K; (a) CO₂ conversion, and (b) CH₄ selectivity.

In this series, the Ni/MgO catalyst turned out to be the best catalyst. However, it must be noted that this catalyst had a higher Ni loading of 31 wt% as compared with the 28 wt% of the Ni/siderite_{reduced}/MgO catalysts. This may be dedicated to the production of the Ni-doped catalysts. The doping of MgO according to the procedure described in Section 3.1 is easier than the doping of (mixed) reduced siderite ore. As a result, a higher loading was achieved, which could not be achieved at all with the mixed catalysts.

To conclude, the study revealed that reduced siderite ore acts as an efficient support material for a Ni-based catalyst for CO₂ methanation when combined with MgO. As expected, the CO₂ conversion increased with increasing Ni loading of the respective catalyst, both for Ni/siderite_{reduced} and Ni/siderite_{reduced}/MgO catalysts, as well as with increasing temperature from 548 K to 648 K, and decreasing feed gas flow rate. When reduced siderite ore was used as sole support material (Ni/siderite_{reduced} catalysts), the catalytic performance (X_{CO₂}, 648 K = 23.0% for 27 wt% Ni/siderite_{reduced}) was only marginally higher than the catalytic performance of undoped reduced siderite ore (X_{CO₂}, 648 K = 19.9%). This leads to the conclusion that both the iron species in and the nickel on the reduced siderite ore show a comparable catalytic effect toward CO₂ hydrogenation. However, the selectivity toward CH₄ is significantly higher when the reduced siderite ore is doped with Ni, specifically, 60.2% compared with 19.0% for undoped reduced siderite ore. This shows the high catalytic activity of the nickel species for CH₄ formation.

With XRD, a NiFe₂³⁺O₄ (trevorite) peak was identified in all Ni/siderite_{reduced} catalysts, as well as the Ni-Fe alloy and FeNi (tetrataenite) in the catalysts after CO₂ hydrogenation (see Section 2.4.2).

However, adding MgO to the support material of the Ni-based catalysts significantly enhanced CO₂ methanation. The ratio of reduced siderite ore and MgO seemed to play a subordinate role, with higher proportions of reduced siderite ore causing slightly higher CO₂ conversions. With ≥50% reduced siderite ore in the mixed siderite_{reduced}/MgO support material, no difference in the catalytic performance was visible anymore. Most importantly, adding MgO to the reduced siderite ore support drastically enhanced the selectivity toward CH₄. Even if only 30% of MgO was present, the selectivity toward methane approached 100%. It can be concluded that with identical Ni loading, Ni/siderite_{reduced}/MgO (≥30% MgO) and Ni/MgO catalysts show comparable catalytic performance, with CO₂ conversions close to the thermodynamic equilibrium and high CH₄ selectivity ≥ 99.9%.

This supports the findings of Loder et al., highlighting the fundamental role of MgO as a basic support material for Ni-based catalysts for CO₂ methanation [9].

2.4. Catalyst Characterization

2.4.1. X-ray Fluorescence Spectrometry

The freshly prepared 24 wt% Ni/siderite_{reduced} catalyst (after calcination, before reduction of NiO to Ni with hydrogen) was analyzed by X-ray fluorescence (XRF) spectrometry for its Ni loading. The Ni loading was compared with the value obtained by AAS analysis. The XRF result showed that NiO was present, and the percentage of Ni (24.81%) was in good agreement with the AAS analysis (24.1%). The other constituents were present at 55.0 wt% Fe₂O₃, 7.45 wt% SiO₂, 2.55 wt% MgO, 1.79 wt% MnO, and 2.31 wt% CaO. This shows that during the wet preparation/impregnation procedure, elemental iron and Fe²⁺ were oxidized to Fe³⁺.

2.4.2. X-ray Diffraction

Fresh and used Ni/siderite_{reduced} catalysts were analyzed by X-ray diffraction (XRD). The Ni-based catalysts on reduced siderite ore support material that were analyzed were (i) 22 wt% Ni/siderite_{reduced} (fresh catalyst), (ii) 22 wt% Ni/siderite_{reduced} (used catalyst), (iii) 24 wt% Ni/siderite_{reduced} (fresh catalyst), (iv) 24 wt% Ni/siderite_{reduced} (used catalyst), (v) 25 wt% Ni/siderite_{reduced} (fresh catalyst), and (vi) 25 wt% Ni/siderite_{reduced} (used catalyst), as shown in Figure 7.

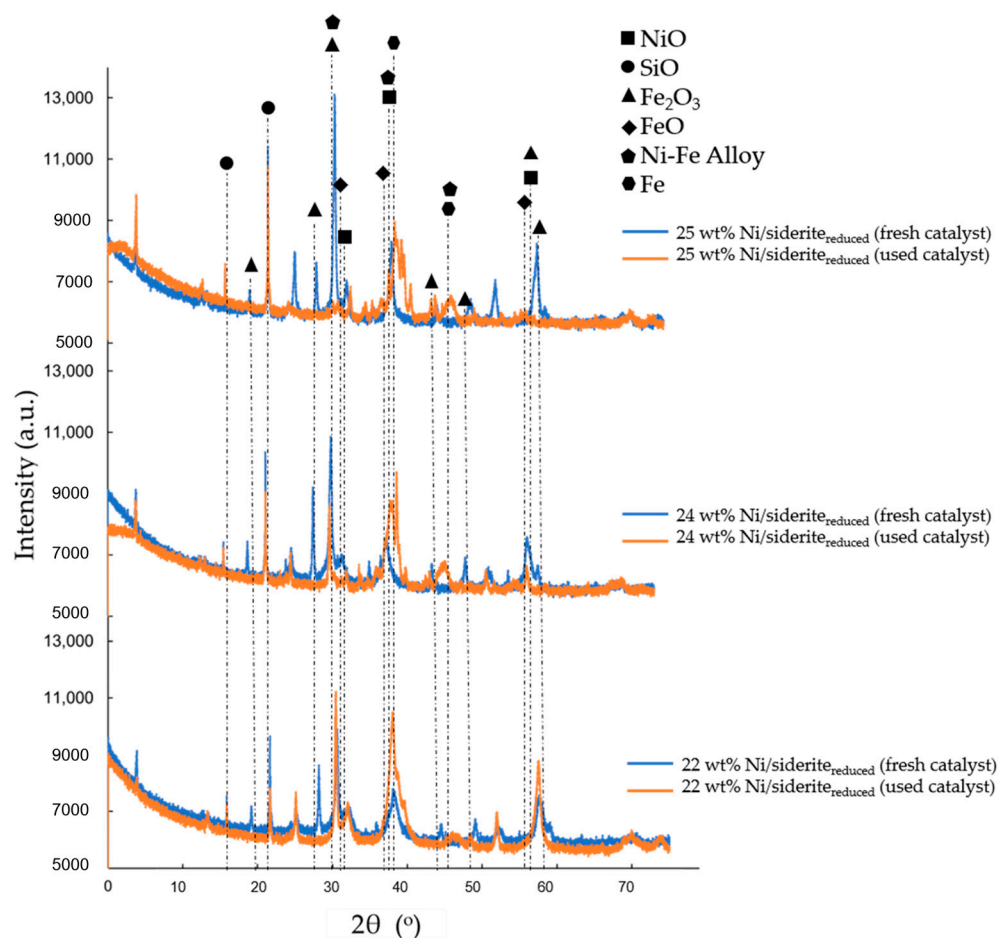


Figure 7. X-ray diffraction results of the fresh and used Ni/siderite_{reduced} catalysts; 22 wt% Ni/siderite_{reduced}, 24 wt% Ni/siderite_{reduced}, and 25 wt% Ni/siderite_{reduced}.

In the fresh Ni/siderite_{reduced} catalysts with 22 wt%, 24 wt%, and 25 wt% Ni loading, the diffraction peaks of NiO (bunsenite), NiFe₂³⁺O₄ (trevorite), Fe₂O₃ (hematite), KAl₂(Si₃Al)O₁₀(OH)₂ (muscovite), SiO₂ (quartz), and FeO (wüstite) were identified. When used for CO₂ hydrogenation, the catalysts changed phases; NiFe₂³⁺O₄ (trevorite) and Fe₂O₃ (hematite) did not appear anymore; nonetheless, Fe²⁺(Fe³⁺)₂O₄ (magnetite), Ni-Fe alloy, and FeNi (tetrataenite) were found in all of the used catalysts (after CO₂ hydrogenation with a molar feed gas ratio H₂:CO₂:N₂ = 56:14:30, feed gas flow rates of 8.02–14.66 m³ kg⁻¹ h⁻¹ (STP), and reaction temperatures of 548 K, 598 K, and 648 K). The result showed that the Ni-Fe alloys were small crystallites with increasing % of Ni. In addition, another iron alloy was found in the 24 wt% Ni/siderite_{reduced} and 25 wt% Ni/siderite_{reduced} catalysts; (Fe,Ni,Co)₃C (cohenite) was present in the catalysts with increased Ni loading. However, the presence of significant quantities of cobalt can be excluded.

2.4.3. Scanning Electron Microscopy (SEM) Analysis

SEM images were taken by Field Emission Scanning Electron Microscopy from the catalyst samples: 21.69 wt% Ni/siderite_{reduced} (Figure 8a), 23.77 wt% Ni/siderite_{reduced} (Figure 8b), 24.80 wt% Ni/siderite_{reduced} (Figure 8c), and 27.71 wt% Ni/siderite_{reduced}/MgO (30:70) (Figure 9a), 28.01 wt% Ni/siderite_{reduced}/MgO (Figure 9b) (50:50), and (c) 28.18 wt% Ni/siderite_{reduced}/MgO (Figure 9c) (70:30).

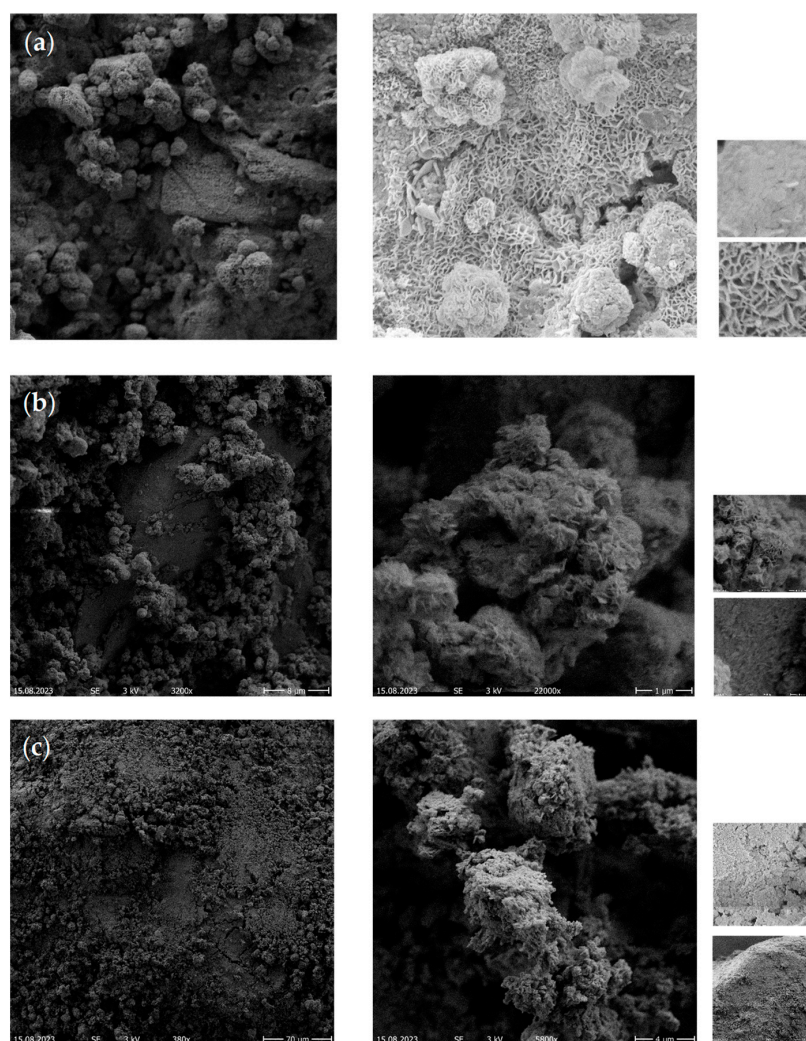


Figure 8. Scanning Electron Microscopy (SEM) analysis of different Ni loadings on the reduced siderite ore support material: (a) 21.69 wt% Ni/siderite_{reduced}, (b) 23.77 wt% Ni/siderite_{reduced}, and (c) 24.80 wt% Ni/siderite_{reduced}; fresh catalysts.

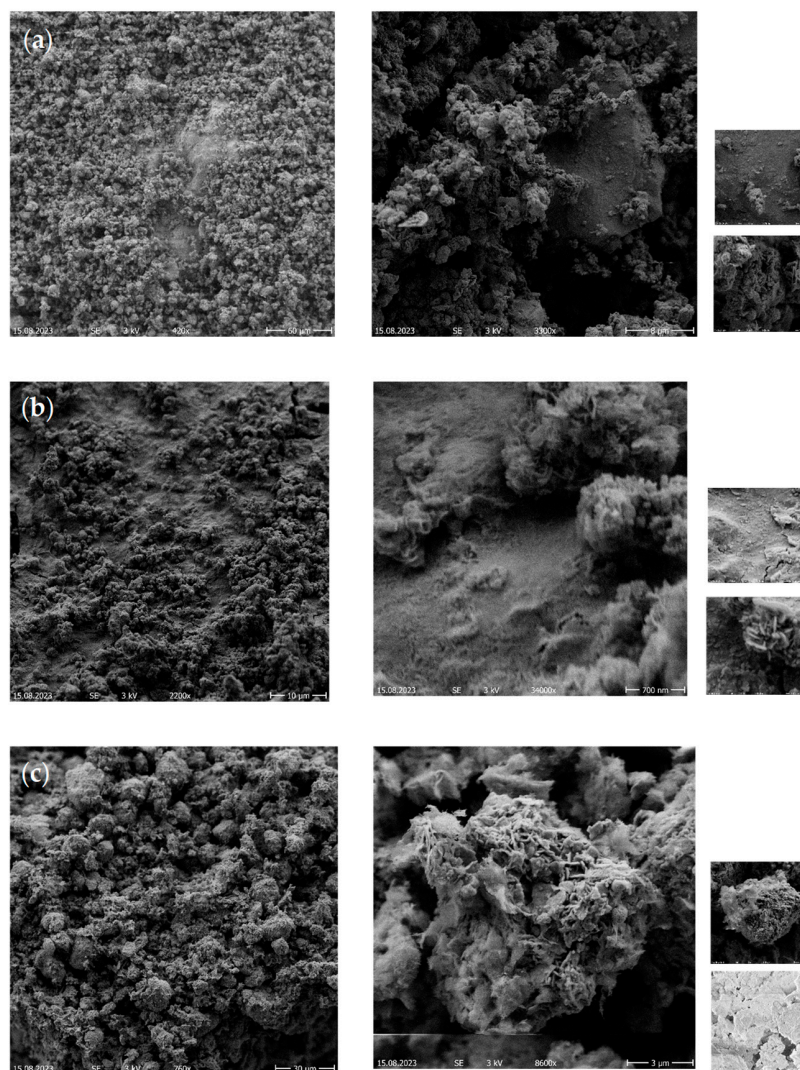


Figure 9. Scanning Electron Microscopy (SEM) analysis of different proportions of reduced siderite ore and MgO as support material for Ni-based catalysts: (a) 27.71 wt% Ni/siderite_{reduced}/MgO (30:70), (b) 28.01 wt% Ni/siderite_{reduced}/MgO, and (c) 28.18 wt% Ni/siderite_{reduced}/MgO.

The SEM images in Figure 8 show that the Ni/siderite_{reduced} catalysts became slick and homogeneous when the Ni loading increased. For all Ni loadings, the particles had a clear distribution of NiO and FeO on the surface. At 21.69 wt% Ni loading, the catalyst had a more porous structure when compared with 23.77 wt% and 24.80 wt% Ni loading on reduced siderite ore. Thus, it can be said that surface morphology changed with increasing Ni loading.

Furthermore, adding MgO to the reduced siderite ore support (siderite_{reduced}:MgO = 30:70, 50:50, 70:30) resulted in more irregularities when increasing the MgO ratio (Figure 9). At siderite_{reduced}:MgO ratios of 30:70 and 50:50, the surface had a flat and homogeneous structure, while the catalyst with the siderite_{reduced}:MgO = 70:30 support had irregular particles on the surface.

3. Materials and Methods

3.1. Materials and Catalyst Preparation

Ni-based catalysts on two different support materials and combinations of the support materials were tested: (i) Ni/MgO, (ii) Ni/siderite_{reduced}, and (iii) Ni/siderite_{reduced}/MgO. The catalysts were prepared by wet impregnation with nickel nitrate hexahydrate (Ni(NO₃)₂ · 6 H₂O, 99%, p.a., Lactan). The MgO support was prepared from MagGran© (4MgCO₃·Mg

(OH)₂·4H₂O), while the siderite ore originated from the Styrian Erzberg, Austria, and was provided by VA Erzberg GmbH, Eisenerz, Austria (particle size 0.5–1 mm). Its mineral composition is given in Table 2.

Table 2. Chemical composition of the original siderite ore determined by XRF spectroscopy [65].

Component	wt%
Fe	33.56
CaO	6.88
MgO	3.72
Mn	1.91
SiO ₂	5.19
Al ₂ O ₃	1.02
others (including CO ₂)	47.72

This siderite ore consists of the iron-bearing minerals siderite ((Fe_{0.83}Mg_{0.11}Mn_{0.05}Ca_{0.01})CO₃) with substitutions of magnesium carbonate (MgCO₃), calcium carbonate (CaCO₃) and manganese carbonate (MnCO₃), and ankerite ((Ca_{0.51}Fe_{0.31}Mg_{0.15}Mn_{0.03})CO₃). Furthermore, dolomite ((Ca,Mg)(CO₃)₂), calcite (CaCO₃), quartz (SiO₂), and muscovite (KAl₂(Al-Si₃O₁₀)(OH)₂) are present in this carbonaceous ore (Table 3).

Table 3. Composition of the original siderite ore from the Austrian Erzberg (particle size 0.5–1 mm) [65].

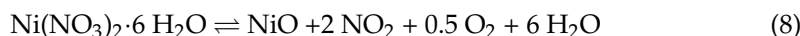
Component	wt%
Siderite	79.04
Calcite	8.91
Quartz	5.19
Ankerite	3.96
Dolomite	1.80
others (including CO ₂)	47.72

The preparation of the catalysts was based on the work of Loder et al. [9] and extended for reduced siderite ore as further catalyst and catalytic support material. There are four main preparation steps:

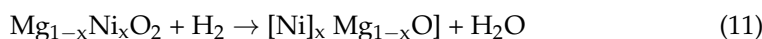
- (i) calcination of magnesium carbonate for magnesium oxide preparation (Equation (6)) and/or reduction of siderite ore (Equation (7)) [69,70],



- (ii) impregnation of the support material with nickel nitrate,
 (iii) thermal decomposition of nickel nitrate to nickel oxide (Equations (8)–(10)) [71], and



- (iv) reduction of Ni with hydrogen (Equations (11) and (12)) [39,71].



The experimental procedure was as follows:

(i) Preparation of the support material:

For magnesium oxide preparation, magnesium carbonate powder ($4 \text{ MgCO}_3 \cdot \text{Mg(OH)}_2 \cdot 4\text{H}_2\text{O}$) was calcined in a muffle furnace (Heraeus M 110) with air at 723 K for 2 h and at 823 K for 5 h.

For preparation of the reduced siderite ore support (for details see Section 3.2), siderite ore was reduced in the tubular reactor used for the methanation experiments, in 90% hydrogen (feed gas ratio of $\text{H}_2:\text{N}_2 = 9:1$, at a feed gas flow rate of $0.048 \text{ m}^3 \text{ h}^{-1}$), and at 773 K and 973 K until the exit gas composition equaled the feed gas composition. The reduced siderite ore was then exposed to air at room temperature, where it partially oxidized.

(ii) Impregnation:

The nickel nitrate solution was prepared from $\text{Ni(NO}_3)_2 \cdot 6 \text{ H}_2\text{O}$ that was mixed with ultrapure water at a nickel concentration of $53\text{--}60 \text{ g dm}^{-3}$ in a flask. After that, the 70 cm^3 nickel solution in the continuously stirred flask was cooled in a water bath ($T = 293\text{--}298 \text{ K}$). 10 g of calcined MgO and/or reduced (and partially oxidized) siderite ore was added to the nickel solution (adding 1 g per 3 min). The mixed solution (slurry phase) was constantly stirred for 2 h and filtrated with the help of a vacuum pump (separated slurry phase and residual water phase). The filtrated slurry (green) phase was dried overnight at room temperature.

(iii) Thermal deposition:

The freshly prepared and pre-dried catalysts were then dried in a muffle furnace (Heraeus M 110) at 393 K for 2 h and at 673 K for 5 h in air. After the drying process, the catalysts had a light gray color.

(iv) Reduction with hydrogen/activation:

This step was required for the reduction of NiO to Ni. A total of 4 g of the catalyst powder was reduced with hydrogen (feed gas ratio of $\text{H}_2:\text{N}_2 = 9:1$, feed gas flow rate of $0.048 \text{ m}^3 \text{ h}^{-1}$) in the tubular reactor at 773 or 973 K (temperature measurement at T_3 thermocouple position, as described in Section 3.4.1, for 4 h.

Then, the catalysts were kept in the tubular reactor and used for the CO_2 methanation experiments.

3.2. Siderite Ore Reduction

The original siderite ore was reduced in a hydrogen atmosphere at two different reduction temperatures, 773 K and 973 K, at ambient pressure and a feed gas ratio of $\text{H}_2:\text{N}_2 = 90:10$. This process step is known as the direct reduction of siderite ore with hydrogen. In the literature, it is suggested for the production of elemental iron from siderite ore in a single process step [65]. The course of the direct reduction process is shown in Figure 10 via the product gas composition at the reactor exit and the reduction temperature at thermocouple position T_3 .

CO and CO_2 formation started in a temperature range of 656–683 K (heat-up phase) for both experiments (final reduction temperatures of 773 K and 973 K, respectively). At 773 K, the highest CO concentration in the product gas was 10.8%, and the highest CO_2 concentration was 37.7% (at the lowest H_2 concentration, 41.9%). At a reduction temperature of 973 K, the highest CO concentration was 13.8%, and the highest CO_2 concentration was found to be 46.4% at the lowest H_2 concentration of 35.3%. In addition, when kept under an inert nitrogen atmosphere, the degree of metallization was 40% and 89% for the reduction temperatures of 773 K and 973 K, respectively.

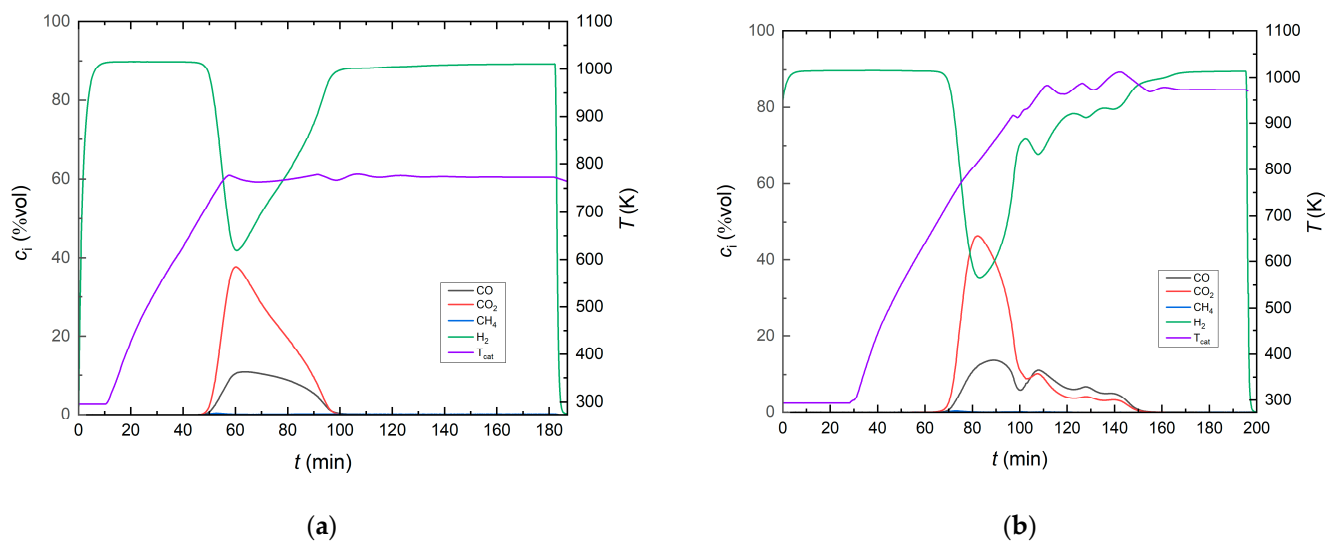
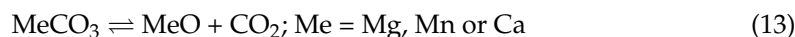


Figure 10. Product gas composition during direct reduction of siderite ore with hydrogen (feed gas ratio $H_2:N_2 = 90:10$, feed gas flow rate $0.048 \text{ m}^3 \text{ h}^{-1}$) for preparation of the support material; (a) $T_{red} = 773 \text{ K}$ and (b) $T_{red} = 973 \text{ K}$.

The concomitant carbonate species in the siderite ore (magnesium, manganese, and calcium carbonate) were converted to their respective bivalent oxides, as shown in Equation (13).



3.3. Catalyst Characterization

3.3.1. X-ray Diffraction

The XRD patterns of the catalyst samples were obtained by a Rigaku SmartLab[®] X-ray diffractometer, Rigaku Corporation, Tokyo, Japan. The samples were collected using a sweep speed of $2.0^\circ \text{ min}^{-1}$ and $2\theta = 5.0\text{--}80.0^\circ$ with a scan step-size of 0.01° .

3.3.2. X-ray Fluorescence Spectrometry

The catalyst samples were dried in a furnace at 378 K for 2 h to determine the loss on ignition (LOI). After that, the samples were mixed with lithium tetraborate ($\text{Li}_2\text{B}_4\text{O}_7$) and lithium metaborate (LiBO_2) and melted in a melting furnace at 1273 K for 1 h . An S8 TIGER Series 2 XRF wavelength dispersive (WDX) spectrometer from Bruker AXS GmbH, Karlsruhe, Germany, was used to determine the catalyst composition using the Best Detection-Vac34mm measurement method.

3.3.3. Scanning Electron Microscopy

The DSM 982 Gemini Field Emission Scanning Electron Microscope (FE-SEM) from Carl Zeiss Microscopy Deutschland GmbH, Oberkochen, Germany, was used to study the surface of the Ni/siderite_{reduced} and Ni/siderite_{reduced}/MgO catalysts. The specimen stage was from -15° to $+90^\circ$, and the working resolution was between 1 and 4 nm . The samples were coated by a single Leica EM ACE600 sputter coater, Leica Mikrosysteme GmbH, Austria.

3.3.4. AAS Analysis

The nickel loading of the catalysts was primarily analyzed by atomic absorption spectrometry (AAS). During the catalyst preparation (impregnation with nickel nitrate), process samples of the nickel solution (before and after impregnation of the support material) were taken and mixed with a solution of $10 \text{ cm}^3 \text{ HNO}_3$ (Carl Roth GmbH, Karlsruhe, Germany) and 990 cm^3 deionized water. An AAnalyst 400 atomic absorption spectrometer (Perkin Elmer Instruments LLC, Shelton, United States of America) was used,

equipped with a nickel hollow cathode lamp set to 25 mA current at a wavelength of 232 nm, and applying a compressed air/ethylene flame, to determine the respective nickel concentrations. From the AAS results, the amount of nickel loading was determined.

3.4. Experimental Setup and Experimental Procedure of the Methanation Experiments

Hydrogen (99.999%), carbon dioxide (99.998%), and nitrogen (99.999%) supplied by Air Liquide were used for the CO₂ hydrogenation experiments. Nitrogen was used as an inert gas for heat transport and balancing purposes.

3.4.1. Experimental Setup

The experimental setup is shown in Figure 11. The feed gases (H₂, CO₂, and N₂) were controlled by three mass flow controllers (MFC1-3). They passed the fixed-bed stainless steel tubular reactor (Parr Instrument GmbH, Illinois, United States of America), which was 0.82 m in length and had an inner diameter of 25 mm. The feed gas stream was preheated by a pre-heating coil (PHC) at the top of the reactor tube before entering the catalyst bed. The tubular reactor was heated by an electric furnace with three heating zones (HT₁–HT₃) at the outer wall of the reactor tube. The temperature in the reactor was measured by six thermocouples (T₁–T₆). They were placed at two positions per heating zone. Stainless steel spacers and a sieve were placed inside the reactor to maintain the catalyst's position. A total of 4 g of the Ni-based catalysts was placed in the middle of the reactor with the thermocouple string (thermocouple diameter = 6 mm) at the lower end of the catalyst bed. When the gas stream had passed the catalyst bed, the gaseous product stream was cooled (i) in the cooler at the outlet of the reactor (HE-1) where the condensate was collected in the condensate trap (CT-1), and (ii) by the gas analyzer cooler (HE-2) with a condensate trap (CT-2) installed to prevent moisture or condensation in the gas analyzer. The dried product gas was sent to the online gas analyzer (GA) consisting of a Caldos27 thermal conductivity analyzer for measuring the hydrogen concentration (measurement ranges: 0–0.5 vol% and 0–100 vol%; output error (2σ): ≤0.5% of smallest measurement range span) and an Uras26 infrared photometer for measuring the CO₂, CO, and CH₄ concentration (measurement ranges: 0–10 vol% and 0–100 vol%; output error (2σ): ≤0.2% of span).

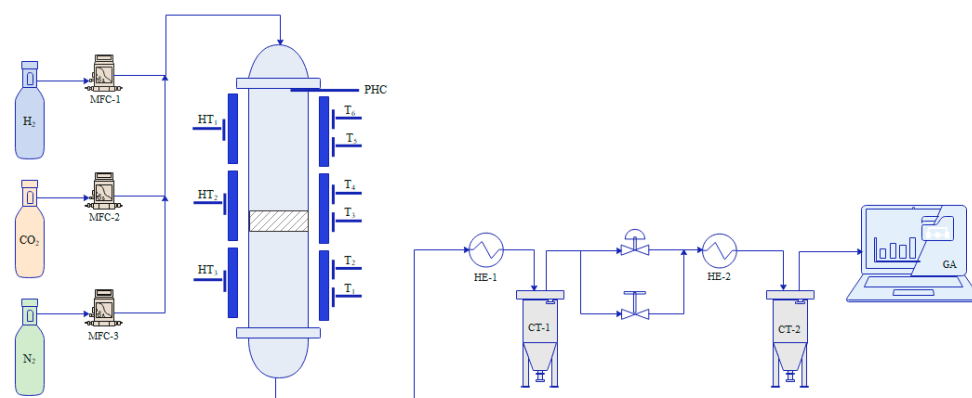


Figure 11. Experimental setup of the tubular reactor used for the CO₂ methanation experiments (MFC: mass flow controller, T₁–T₆: thermocouple inside the reactor tube, HT₁–HT₃, temperature measurement position in the middle of a heating zone, PHC: pre-heating coil, HE: heat exchanger, CT: condensate tank, BPR: back pressure regulator, GA: gas analyzer).

3.4.2. Experimental Procedure

CO₂ methanation experiments were performed at ambient pressure, feed gas flow rates of 8.02–14.66 m³ kg^{−1} h^{−1} (STP), and a constant volumetric feed gas ratio (H₂:CO₂:N₂ = 56:14:30). According to Sommerbauer et al. [72], preliminary temperature scanning tests were conducted for each catalyst to evaluate the characteristic temperature effects of the respective catalyst regarding CO₂ conversion and methane selectivity before proceeding to

steady-state experiments. Therefore, the reaction temperature range was set to 548–623 K. 4 g of the catalyst sample was used for each experiment. It was placed in the middle of the reactor tube. Pure nitrogen was used for purging the system at ambient temperature and pressure, and the composition was checked by the online gas analyzer. Next, the feed gas stream ($\text{H}_2:\text{CO}_2:\text{N}_2 = 56:14:30$) with the designed feed gas flow rate was fed to the reactor while the heater was heated to the target temperature, which was measured at the end of the catalyst bed ($T_{\text{cat}} = T_3$). The gaseous products in the product gas stream were analyzed by the online gas analyzer after passing two heat exchangers for condensation of water. The dry gaseous product stream consisted of N_2 , CO , CO_2 , CH_4 , and H_2 only. There were no other constituents present in the dry product gas (at concentrations exceeding 0.1 vol%).

The performance of the catalysts was evaluated with regard to CO_2 conversion (X_{CO_2} , Equation (14)) and CH_4 selectivity (S_{CH_4} , Equation (15)), with $c_{\text{CO}_2,0}$ being the initial concentration of CO_2 and c_i being the concentration of any species i at the outlet of the reactor. The volumetric expansion coefficient $\varepsilon_{\text{CO}_2}$ was calculated by Equation (16), with $y_{\text{CO}_2,0}$ being the molar feed fraction of CO_2 and the stoichiometric coefficients of the methanation reactions a , b , c , and d (CO_2 : $a = -1$, H_2 : $b = -4$, CH_4 : $c = 1$, and H_2O : $d = 2$). The concentrations of the species (c_{N_2} , c_{H_2} and the product concentration c_P for the products CH_4 and CO , respectively) were calculated with Equations (17)–(19).

$$X_{\text{CO}_2} = \frac{c_{\text{CO}_2,0} - c_{\text{CO}_2}}{c_{\text{CO}_2,0} + \varepsilon_{\text{CO}_2} \cdot c_{\text{CO}_2}} \quad (14)$$

$$S_{\text{CH}_4} = \frac{c_{\text{CH}_4}}{c_{\text{CH}_4} + c_{\text{CO}_2}} \quad (15)$$

$$\varepsilon_{\text{CO}_2} = y_{\text{CO}_2,0} \cdot \left(\frac{|c|}{|a|} + \frac{|d|}{|a|} - \frac{|b|}{|a|} - 1 \right) \quad (16)$$

$$c_{\text{N}_2} = \frac{c_{\text{N}_2,0}}{1 + \varepsilon_{\text{CO}_2} \cdot X_{\text{CO}_2}} \quad (17)$$

$$c_{\text{H}_2} = \frac{c_{\text{H}_2,0} - b \cdot X_{\text{CO}_2} \cdot c_{\text{CO}_2,0}}{1 + \varepsilon_{\text{CO}_2} \cdot X_{\text{CO}_2}} \quad (18)$$

$$c_P = \frac{(|c| \text{ or } |d|) \cdot X_{\text{CO}_2} \cdot c_{\text{CO}_2,0}}{1 + \varepsilon_{\text{CO}_2} \cdot X_{\text{CO}_2}} \quad (19)$$

3.4.3. Determination of the Chemical Composition of the Reduced Siderite Ore

The chemical composition of the reduced siderite ore was characterized in a five step analysis procedure at the Chair of Mineral Processing, Montanuniversität Leoben:

- (i) Measurement of the weight increase in air (equaling the reactivity of the sample in air) and determination of the oxidation state by loss on ignition (LOI, fully oxidized and in a neutral atmosphere);
- (ii) Combustion analysis via the Leco method to determine the total (residual) carbon content;
- (iii) Selective dissolution of metallic iron from iron oxides in bromine/methanol to determine elemental iron and for the determination of dissolved iron as Fe^{II} via the Zimmermann–Reinhardt method;
- (iv) Digestion of the filter cake in boiling hydrochloric acid (HCl) to determine bivalent Fe^{II} and trivalent Fe^{III} iron using the Zimmermann–Reinhardt method;
- (v) X-ray diffraction of the residual elements.

The degree of metallization (w_{met}) is defined as the mass of elemental iron (m_{Fe}^0) with respect to the total mass of iron-bearing components in the reduced iron ore ($m_{\text{Fe,tot}}$).

4. Conclusions

In this study, the catalytic potential of hydrogen-reduced siderite ore, and Ni-based catalysts on reduced siderite ore and mixed reduced siderite ore/MgO support material was evaluated. It was shown that siderite ore that was reduced in a hydrogen atmosphere can act as a CO₂ hydrogenation catalyst but only causes low selectivity toward CH₄. Ni-based catalysts on reduced siderite ore only showed marginally higher catalytic activity than undoped reduced siderite ore. However, it was proven that MgO plays a fundamental role as a basic support material for Ni-based CO₂ methanation catalysts by drastically enhancing both CO₂ conversion and selectivity toward CH₄. When MgO was present in the support material, even fractions as low as 30% resulted in CO₂ conversions close to the thermodynamic equilibrium and CH₄ selectivities of at least 95% (mainly $\geq 99.9\%$). It could be shown that reduced siderite ore itself shows minor catalytic activity for CO₂ methanation but, in combination with MgO, has a clear synergistic effect as a support material for Ni-based catalysts giving access to highly efficient CO₂ methanation catalysts

Author Contributions: Conceptualization, S.L. and K.S.; methodology, S.L. and K.S.; validation, K.S.; formal analysis, K.S.; investigation, K.S.; resources, S.L.; data curation, K.S. and S.S.; writing—original draft preparation, K.S. and S.L.; writing—review and editing, S.L. and C.A.H.; visualization, K.S.; supervision, S.L.; project administration, S.L.; funding acquisition, K.S. and S.L. All authors have read and agreed to the published version of the manuscript.

Funding: This research was funded by Zukunftsfonds Steiermark, grant number 1481. Open Access Funding by the Graz University of Technology.

Data Availability Statement: The data presented in this study are available on request from the corresponding author.

Acknowledgments: The authors acknowledge financial support from NAWI Graz. The analytical equipment data was supported by Michael Gostencnik, Department of Earth Sciences—NAWI Graz Geocenter, University of Graz. Special thanks go to Alfred Stadtschnitzer from VA Erzberg GmbH for providing the siderite ore. Publication was supported by TU Graz Open Access Publishing Fund.

Conflicts of Interest: The authors declare no conflicts of interest. The funders had no role in the design of the study; in the collection, analyses, or interpretation of data; in the writing of the manuscript; or in the decision to publish the results.

References

1. Wei, W.; Jinlong, G. Methanation of carbon dioxide: An overview. *Front. Chem. Sci. Eng.* **2011**, *5*, 2–10. [[CrossRef](#)]
2. Aziz, M.A.A.; Jalil, A.A.; Triwahyono, S.; Ahmad, A. CO₂ methanation over heterogeneous catalysts: Recent progress and future prospects. *Green Chem.* **2015**, *17*, 2647–2663. [[CrossRef](#)]
3. Hao, W.; Vall, M.; Shi, Y.; Wang, Q.; Strømme, M.; Yan, X.; Cheung, O.; Li, R. Novel Ni/MgO Catalysts from Mesoporous MgCO₃ for Highly Efficient CO Methanation: Effects of Al and Si Stabilization. *ChemRxiv* 2020. *preprint*.
4. Park, S.-E.; Yoo, J.S. New CO₂ chemistry—Recent advances in utilizing CO₂ as an oxidant and current understanding on its role. Carbon Dioxide Utilization for Global Sustainability. In Proceedings of the 7th International Conference on Carbon Dioxide Utilization, Seoul, Republic of Korea, 12–16 October 2004; Elsevier: Amsterdam, The Netherlands, 2004; pp. 303–314.
5. Downing, C.A.; Sokol, A.A.; Catlow, C.R.A. The reactivity of CO₂ on the MgO(100) surface. *Phys. Chem. Chem. Phys.* **2014**, *16*, 184–195. [[CrossRef](#)] [[PubMed](#)]
6. Pandey, D.; Ray, K.; Bhardwaj, R.; Bojja, S.; Chary, K.; Deo, G. Promotion of unsupported nickel catalyst using iron for CO₂ methanation. *Int. J. Hydrog. Energy* **2018**, *43*, 4987–5000. [[CrossRef](#)]
7. Yin, L.; Chen, X.; Sun, M.; Zhao, B.; Chen, J.; Zhang, Q.; Ning, P. Insight into the role of Fe on catalytic performance over the hydrotalcite-derived Ni-based catalysts for CO₂ methanation reaction. *Int. J. Hydrog. Energy* **2022**, *47*, 7139–7149. [[CrossRef](#)]
8. Huynh, H.L.; Zhu, J.; Zhang, G.; Shen, Y.; Tucho, W.M.; Ding, Y.; Yu, Z. Promoting effect of Fe on supported Ni catalysts in CO₂ methanation by in situ DRIFTS and DFT study. *J. Catal.* **2020**, *392*, 266–277. [[CrossRef](#)]
9. Loder, A.; Siebenhofer, M.; Lux, S. The reaction kinetics of CO₂ methanation on a bifunctional Ni/MgO catalyst. *J. Ind. Eng. Chem.* **2020**, *85*, 196–207. [[CrossRef](#)]
10. Beuls, A.; Swalus, C.; Jacquemin, M.; Heyen, G.; Karelavic, A.; Ruiz, P. Methanation of CO₂: Further insight into the mechanism over Rh/ γ -Al₂O₃ catalyst. *Appl. Catal. B Environ.* **2012**, *113–114*, 2–10. [[CrossRef](#)]
11. Brooks, K.P.; Hu, J.; Zhu, H.; Kee, R.J. Methanation of carbon dioxide by hydrogen reduction using the Sabatier process in microchannel reactors. *Chem. Eng. Sci.* **2007**, *62*, 1161–1170. [[CrossRef](#)]

12. Pan, Q.; Peng, J.; Sun, T.; Wang, S.; Wang, S. Insight into the reaction route of CO₂ methanation: Promotion effect of medium basic sites. *Catal. Commun.* **2014**, *45*, 74–78. [[CrossRef](#)]
13. Aldana, P.U.; Ocampo, F.; Kobl, K.; Louis, B.; Thibault-Starzyk, F.; Daturi, M.; Bazin, P.; Thomas, S.; Roger, A.C. Catalytic CO₂ valorization into CH₄ on Ni-based ceria-zirconia. Reaction mechanism by operando IR spectroscopy. *Catal. Today* **2013**, *215*, 201–207. [[CrossRef](#)]
14. Ge, F.; Zhu, J.; Du, X.; Wang, P.; Chen, Y.; Zhuang, W.; Song, M.; Sun, L.; Tao, X.; Li, J.; et al. Constructing the highly efficient Ni/ZrO₂/SiO₂ catalyst by a combustion-impregnation method for low-temperature CO₂ methanation. *J. Environ. Chem. Eng.* **2022**, *10*, 108476. [[CrossRef](#)]
15. Xu, Y.; Wan, H.; Du, X.; Yao, B.; Wei, S.; Chen, Y.; Zhuang, W.; Yang, H.; Sun, L.; Tao, X.; et al. Highly active Ni/CeO₂/SiO₂ catalyst for low-temperature CO₂ methanation: Synergistic effect of small Ni particles and optimal amount of CeO₂. *Fuel Process. Technol.* **2022**, *236*, 107418. [[CrossRef](#)]
16. Aziz, M.; Jalil, A.A.; Triwahyono, S.; Mukti, R.R.; Taufiq-Yap, Y.H.; Sazegar, M.R. Highly active Ni-promoted mesostructured silica nanoparticles for CO₂ methanation. *Appl. Catal. B Environ.* **2014**, *147*, 359–368. [[CrossRef](#)]
17. Ren, J.; Guo, H.; Yang, J.; Qin, Z.; Lin, J.; Li, Z. Insights into the mechanisms of CO₂ methanation on Ni(111) surfaces by density functional theory. *Appl. Surf. Sci.* **2015**, *351*, 504–516. [[CrossRef](#)]
18. Shen, L.; Xu, J.; Zhu, M.; Han, Y.-F. Essential Role of the Support for Nickel-Based CO₂ Methanation Catalysts. *ACS Catal.* **2020**, *10*, 14581–14591. [[CrossRef](#)]
19. Zhou, G.; Liu, H.; Xing, Y.; Xu, S.; Xie, H.; Xiong, K. CO₂ hydrogenation to methane over mesoporous Co/SiO₂ catalysts: Effect of structure. *J. CO₂ Util.* **2018**, *26*, 221–229. [[CrossRef](#)]
20. Da Silva, D.C.; Letichevsky, S.; Borges, L.E.; Appel, L.G. The Ni/ZrO₂ catalyst and the methanation of CO and CO₂. *Int. J. Hydrog. Energy* **2012**, *37*, 8923–8928. [[CrossRef](#)]
21. Jia, X.; Zhang, X.; Rui, N.; Hu, X.; Liu, C. Structural effect of Ni/ZrO₂ catalyst on CO₂ methanation with enhanced activity. *Appl. Catal. B Environ.* **2019**, *244*, 159–169. [[CrossRef](#)]
22. Kim, H.Y.; Lee, H.M.; Park, J.-N. Bifunctional mechanism of CO₂ methanation on Pd-MgO/SiO₂ catalyst: Independent roles of MgO and Pd on CO₂ methanation. *J. Phys. Chem. C* **2010**, *114*, 7128–7131. [[CrossRef](#)]
23. Zhang, T.; Liu, Q. Mesostructured cellular foam silica supported bimetallic LaNi_{1-x}Co_xO₃ catalyst for CO₂ methanation. *Int. J. Hydrog. Energy* **2020**, *45*, 4417–4426. [[CrossRef](#)]
24. Yuan, H.; Zhu, X.; Han, J.; Wang, H.; Ge, Q. Rhenium-promoted selective CO₂ methanation on Ni-based catalyst. *J. CO₂ Util.* **2018**, *26*, 8–18. [[CrossRef](#)]
25. Tada, S.; Shimizu, T.; Kameyama, H.; Haneda, T.; Kikuchi, R. Ni/CeO₂ catalysts with high CO₂ methanation activity and high CH₄ selectivity at low temperatures. *Int. J. Hydrog. Energy* **2012**, *37*, 5527–5531. [[CrossRef](#)]
26. Song, M.; Shi, L.; Xu, X.; Du, X.; Chen, Y.; Zhuang, W.; Tao, X.; Sun, L.; Xu, Y. Ni/M/SiO₂ catalyst (M=La, Ce or Mg) for CO₂ methanation: Importance of the Ni active sites. *J. CO₂ Util.* **2022**, *64*, 102150. [[CrossRef](#)]
27. Huang, J.; Li, X.; Wang, X.; Fang, X.; Wang, H.; Xu, X. New insights into CO₂ methanation mechanisms on Ni/MgO catalysts by DFT calculations: Elucidating Ni and MgO roles and support effects. *J. CO₂ Util.* **2019**, *33*, 55–63. [[CrossRef](#)]
28. Rahmani, S.; Rezaei, M.; Meshkani, F. Preparation of highly active nickel catalysts supported on mesoporous nanocrystalline γ-Al₂O₃ for CO₂ methanation. *J. Ind. Eng. Chem.* **2014**, *20*, 1346–1352. [[CrossRef](#)]
29. Xu, Y.; Wu, Y.; Li, J.; Wei, S.; Gao, X.; Wang, P. Combustion-impregnation preparation of Ni/SiO₂ catalyst with improved low-temperature activity for CO₂ methanation. *Int. J. Hydrog. Energy* **2021**, *46*, 20919–20929. [[CrossRef](#)]
30. Frontera, P.; Macario, A.; Ferraro, M.; Antonucci, P. Supported Catalysts for CO₂ Methanation: A Review. *Catalysts* **2017**, *7*, 59. [[CrossRef](#)]
31. Perkas, N.; Amirian, G.; Zhong, Z.; Teo, J.; Gofer, Y.; Gedanken, A. Methanation of Carbon Dioxide on Ni Catalysts on Mesoporous ZrO₂ Doped with Rare Earth Oxides. *Catal. Lett.* **2009**, *130*, 455–462. [[CrossRef](#)]
32. Yamasaki, M.; Habazaki, H.; Asami, K.; Izumiya, K.; Hashimoto, K. Effect of tetragonal ZrO₂ on the catalytic activity of Ni/ZrO₂ catalyst prepared from amorphous Ni–Zr alloys. *Catal. Commun.* **2006**, *7*, 24–28. [[CrossRef](#)]
33. Nakayama, T.; Ichikuni, N.; Sato, S.; Nozaki, F. Ni/MgO catalyst prepared using citric acid for hydrogenation of carbon dioxide. *Appl. Catal. A Gen.* **1997**, *158*, 185–199. [[CrossRef](#)]
34. Bette, N.; Thielemann, J.; Schreiner, M.; Mertens, F. Methanation of CO₂ over a (Mg,Al)O_x Supported Nickel Catalyst Derived from a (Ni,Mg,Al)-Hydrotalcite-like Precursor. *ChemCatChem* **2016**, *8*, 2903–2906. [[CrossRef](#)]
35. Fedoročková, A.; Raschman, P. Effects of pH and acid anions on the dissolution kinetics of MgO. *Chem. Eng. J.* **2008**, *143*, 265–272. [[CrossRef](#)]
36. Ho, K.; Jin, S.; Zhong, M.; Vu, A.-T.; Lee, C.-H. Sorption capacity and stability of mesoporous magnesium oxide in post-combustion CO₂ capture. *Mater. Chem. Phys.* **2017**, *198*, 154–161. [[CrossRef](#)]
37. Takezawa, N.; Terunuma, H.; Shimokawabe, M.; Kobayashib, H. Methanation of carbon dioxide: Preparation of Ni/MgO catalysts and their performance. *Appl. Catal.* **1986**, *23*, 291–298. [[CrossRef](#)]
38. Varun, Y.; Sreedhar, I.; Singh, S.A. Highly stable M/NiO–MgO (M = Co, Cu and Fe) catalysts towards CO₂ methanation. *Int. J. Hydrog. Energy* **2020**, *45*, 28716–28731. [[CrossRef](#)]
39. Baldauf-Sommerbauer, G.; Lux, S.; Aniser, W.; Bitschnau, B.; Letofsky-Papst, I.; Siebenhofer, M. Steady-state and controlled heating rate methanation of CO₂ on Ni/MgO in a bench-scale fixed bed tubular reactor. *J. CO₂ Util.* **2018**, *23*, 1–9. [[CrossRef](#)]

40. Suksumrit, K.; Kleiber, S.; Lux, S. The Role of Carbonate Formation during CO₂ Hydrogenation over MgO-Supported Catalysts: A Review on Methane and Methanol Synthesis. *Energies* **2023**, *16*, 2973. [[CrossRef](#)]
41. Pandey, D.; Deo, G. Promotional effects in alumina and silica supported bimetallic Ni–Fe catalysts during CO₂ hydrogenation. *J. Mol. Catal. A Chem.* **2014**, *382*, 23–30. [[CrossRef](#)]
42. Franken, T.; Heel, A. Are Fe based catalysts an upcoming alternative to Ni in CO₂ methanation at elevated pressure? *J. CO₂ Util.* **2020**, *39*, 101175. [[CrossRef](#)]
43. Sehested, J.; Larsen, K.E.; Kustov, A.L.; Frey, A.M.; Johannessen, T.; Bligaard, T.; Andersson, M.P.; Nørskov, J.K.; Christensen, C.H. Discovery of technical methanation catalysts based on computational screening. *Top. Catal.* **2007**, *45*, 9–13. [[CrossRef](#)]
44. Mutz, B.; Belimov, M.; Wang, W.; Sprenger, P.; Serrer, M.-A.; Wang, D.; Pfeifer, P.; Kleist, W.; Grunwaldt, J.-D. Potential of an Alumina-Supported Ni₃Fe Catalyst in the Methanation of CO₂: Impact of Alloy Formation on Activity and Stability. *ACS Catal.* **2017**, *7*, 6802–6814. [[CrossRef](#)]
45. Serrer, M.-A.; Kalz, K.F.; Saraçi, E.; Lichtenberg, H.; Grunwaldt, J.-D. Role of Iron on the Structure and Stability of Ni_{3.2}Fe/Al₂O₃ during Dynamic CO₂ Methanation for P2X Applications. *ChemCatChem* **2019**, *11*, 5018–5021. [[CrossRef](#)]
46. Mebrahtu, C.; Krebs, F.; Perathoner, S.; Abate, S.; Centi, G.; Palkovits, R. Hydrotalcite based Ni–Fe/(Mg,Al)O_x catalysts for CO₂ methanation—Tailoring Fe content for improved CO dissociation, basicity, and particle size. *Catal. Sci. Technol.* **2018**, *8*, 1016–1027. [[CrossRef](#)]
47. Wang, G.; Xu, S.; Jiang, L.; Wang, C. Nickel supported on iron-bearing olivine for CO₂ methanation. *Int. J. Hydrog. Energy* **2016**, *41*, 12910–12919. [[CrossRef](#)]
48. Ram Reddy, M.K.; Xu, Z.P.; Da Diniz Costa, J.C. Influence of water on high-temperature CO₂ capture using layered double hydroxide derivatives. *Ind. Eng. Chem. Res.* **2008**, *47*, 2630–2635. [[CrossRef](#)]
49. Ratchahat, S.; Sudoh, M.; Suzuki, Y.; Kawasaki, W.; Watanabe, R.; Fukuhara, C. Development of a powerful CO₂ methanation process using a structured Ni/CeO₂ catalyst. *J. CO₂ Util.* **2018**, *24*, 210–219. [[CrossRef](#)]
50. Moghaddam, S.V.; Rezaei, M.; Meshkani, F.; Daroughegi, R. Synthesis of nanocrystalline mesoporous Ni/Al₂O₃ single bond SiO₂ catalysts for CO₂ methanation reaction. *Int. J. Hydrog. Energy* **2018**, *43*, 19038–19046. [[CrossRef](#)]
51. Hu, L.; Urakawa, A. Continuous CO₂ capture and reduction in one process: CO₂ methanation over unpromoted and promoted Ni/ZrO₂. *J. CO₂ Util.* **2018**, *25*, 323–329. [[CrossRef](#)]
52. Hwang, S.; Hong, U.G.; Lee, J.; Seo, J.G.; Baik, J.H.; Koh, D.J.; Lim, H.; Song, I.K. Methanation of carbon dioxide over mesoporous Ni–Fe–Al₂O₃ catalysts prepared by a coprecipitation method: Effect of precipitation agent. *J. Ind. Eng. Chem.* **2013**, *19*, 2016–2021. [[CrossRef](#)]
53. Zhang, Y.; Chen, Y.; Liu, Q. Green synthesis of MCM-41 derived from renewable biomass and construction of VO_x-modified nickel phyllosilicate catalyst for CO₂ methanation. *Int. J. Hydrog. Energy* **2021**, *46*, 32003–32016. [[CrossRef](#)]
54. Gao, W.; Meng, X.; Jin, D.; Xu, B.; Dai, W.; Zhao, R.; Xin, Z. Polyol-pretreated SBA-16 supported Ni-Fe bimetallic catalyst applied in CO methanation at low temperature. *Mol. Catal.* **2021**, *512*, 111769. [[CrossRef](#)]
55. González-Castaño, M.; Navarro de Miguel, J.C.; Boelte, J.-H.; Centeno, M.A.; Klepel, O.; Arellano-García, H. Assessing the impact of textural properties in Ni–Fe catalysts for CO₂ methanation performance. *Microporous Mesoporous Mater.* **2021**, *327*, 111405. [[CrossRef](#)]
56. Kirchner, J.; Anolleck, J.K.; Lösch, H.; Kureti, S. Methanation of CO₂ on iron based catalysts. *Appl. Catal. B Environ.* **2018**, *223*, 47–59. [[CrossRef](#)]
57. Kumar Prabhakar, J.; Apte, P.A.; Deo, G. The kinetics of Ni/Al₂O₃ and Ni-Fe/Al₂O₃ catalysts for the CO₂ methanation reaction and the reasons for promotion. *Chem. Eng. J.* **2023**, *471*, 144252. [[CrossRef](#)]
58. Lan, P.-W.; Wang, C.-C.; Chen, C.-Y. Effect of Ni/Fe ratio in Ni–Fe catalysts prepared under external magnetic field on CO₂ methanation. *J. Taiwan Inst. Chem. Eng.* **2021**, *127*, 166–174. [[CrossRef](#)]
59. Tsuji, M.; Kodama, T.; Yoshida, T.; Kitayama, Y.; Tamaura, Y. Preparation and CO₂ methanation activity of an ultrafine Ni(II) ferrite catalyst. *J. Catal.* **1996**, *164*, 315–321. [[CrossRef](#)]
60. Bel Hadjltaief, H.; Sdiri, A.; Gálvez, M.; Zidi, H.; Da Costa, P.; Ben Zina, M. Natural Hematite and Siderite as Heterogeneous Catalysts for an Effective Degradation of 4-Chlorophenol via Photo-Fenton Process. *ChemEngineering* **2018**, *2*, 29. [[CrossRef](#)]
61. Wei, Y.; Gui, K.; Liu, X.; Liang, H.; Gu, S.; Ren, D. Performance of Mn-Ce co-doped siderite catalysts in the selective catalytic reduction of NO_x by NH₃. *J. Fuel Chem. Teshimachnol.* **2019**, *47*, 1495–1503. [[CrossRef](#)]
62. Görmez, Ö.; Saçlı, B.; Çağlayan, U.; Kalderis, D.; Gözmen, B. Hydrothermal Synthesis of Siderite and Application as Catalyst in the Electro-Fenton Oxidation of *p*-Benzoquinone. *Molecules* **2022**, *27*, 8056. [[CrossRef](#)]
63. Boehm, A.; Boehm, M.; Kogelbauer, A. Neutrons for Mineral Processing—Thermo Diffractometry to Investigate Mineral Selective Magnetizing Flash Roasting. *Chem. Ing. Tech.* **2014**, *86*, 883–890. [[CrossRef](#)]
64. Lin, G.; Zhang, L.; Peng, J.; Hu, T.; Yang, L. Microwave roasting of siderite and the catalytic combustion effects on anthracite. *Appl. Therm. Eng.* **2017**, *117*, 668–674. [[CrossRef](#)]
65. Loder, A.; Siebenhofer, M.; Böhm, A.; Lux, S. Clean iron production through direct reduction of mineral iron carbonate with low-grade hydrogen sources; the effect of reduction feed gas composition on product and exit gas composition. *Clean. Eng. Technol.* **2021**, *5*, 100345. [[CrossRef](#)]
66. Loder, A.; Santner, S.; Siebenhofer, M.; Böhm, A.; Lux, S. Reaction kinetics of direct reduction of mineral iron carbonate with hydrogen: Determination of the kinetic triplet. *Chem. Eng. Res. Des.* **2022**, *188*, 575–589. [[CrossRef](#)]

67. Lux, S.; Baldauf-Sommerbauer, G.; Ottitsch, B.; Loder, A.; Siebenhofer, M. Iron Carbonate Beneficiation Through Reductive Calcination-Parameter Optimization to Maximize Methane Formation. *Eur. J. Inorg. Chem.* **2019**, *2019*, 1748–1758. [[CrossRef](#)]
68. Bock, S.; Pauritsch, M.; Lux, S.; Hacker, V. Natural iron ores for large-scale thermochemical hydrogen and energy storage. *Energy Convers. Manag.* **2022**, *267*, 115834. [[CrossRef](#)]
69. Lux, S.; Baldauf-Sommerbauer, G.; Siebenhofer, M. Hydrogenation of Inorganic Metal Carbonates: A Review on Its Potential for Carbon Dioxide Utilization and Emission Reduction. *ChemSusChem* **2018**, *11*, 3357–3375. [[CrossRef](#)]
70. Reller, A.; Emmenegger, R.; Padeste, C.; Oswald, H.-R. Thermochemical Reactivity of Metal Carbonates. *Chimia* **1991**, *45*, 262. [[CrossRef](#)]
71. Kleiber, S.; Loder, A.; Siebenhofer, M.; Böhm, A.; Lux, S. Direct reduction of siderite ore combined with catalytic CO/CO₂ hydrogenation to methane and methanol: A technology concept. *Chem. Ing. Tech.* **2022**, *94*, 701–711. [[CrossRef](#)]
72. Baldauf-Sommerbauer, G.; Lux, S.; Wagner, J.; Siebenhofer, M. Determination of the kinetic triplet by an isoconversional and a regression method applied to the decomposition of mineral iron carbonate in nitrogen. *Thermochim. Acta* **2017**, *649*, 1–12. [[CrossRef](#)]

Disclaimer/Publisher’s Note: The statements, opinions and data contained in all publications are solely those of the individual author(s) and contributor(s) and not of MDPI and/or the editor(s). MDPI and/or the editor(s) disclaim responsibility for any injury to people or property resulting from any ideas, methods, instructions or products referred to in the content.